Non-Volatility Property and Pinched Hysteresis Loops of 2-terminal Devices and Memristors

Makoto Itoh [1]
1-19-20-203, Arae, Jonan-ku,
Fukuoka, 814-0101 JAPAN
Email: itoh-makoto@jcom.home.ne.jp

Abstract
It is well known that memristors can be classified into the four classes according to the complexity of their mathematical representation. Furthermore, the four classes of memristors are used to qualitatively simulate many of the experimentally measured pinched hysteresis loops. In this paper, we define the 2-terminal devices, which do not belong to the above four classes of memristors, but have the same non-volatile property as the ideal memristor. We then study the non-volatile mechanism of these devices and the memristors that can retain the previous value of the state even when the driving signal is set to zero. We show that the ideal generic memristors and the generalized 2-terminal devices can have interesting applications: non-volatile multi-valued memories and two-element chaotic oscillators, if we remove the condition that no state change occurs after the zero driving signal. We also show that the 2-terminal devices and the four classes of memristors can exhibit a wide variety of pinched hysteresis loops similar to those measured experimentally. Furthermore, we show that a wide variety of Lissajous curves are possible, depending on whether the direction of the Lissajous curve is clockwise or counterclockwise and which quadrants the Lissajous curve passes through.

Keywords
memristor; memristive device; 2-terminal device; non-volatility; pinched hysteresisloop; Lissajous curve; non-volatile multiple-valued memory; reconstruction method; Duffing oscillator; Josephson junction circuit; Mathieu equation.

1 Introduction

A number of experimentally measured pinched hysteresis loops are shown in [1], which are extracted from dozens of literature. These pinched hysteresis loops are made of different materials, processes, and physical mechanisms [1]. It is well known that memristors are classified into the four classes according to the complexity of their mathematical representation [2]. Furthermore, many of the experimentally measured pinched hysteresis loops are qualitatively simulated using the four classes of memristors [1, 2, 3].

In this paper, we define the 2-terminal devices, which do not belong to the above four classes of memristors, but have the same non-volatile property as the ideal memristor. We then study the non-volatile mechanism of these devices and memristors, which can maintain the previous value of the state even when the driving signal is set to zero. We also show that the 2-terminal devices and the four classes of memristors can exhibit a wide variety of pinched hysteresis loops similar to those measured experimentally. Furthermore, we show that a wide variety of Lissajous curves are possible, depending on whether the direction of the Lissajous curve is clockwise or counterclockwise and which quadrants the Lissajous curve passes

[1] Since his retirement in 2010, he has continued to study the nonlinear dynamics of memristors.

through. Finally, we study the case where the state evolves with time even when the drive signal is set to zero. That is, we remove the condition that no state change occurs after the drive signal is zero. In this case, the ideal generic memristors and the generalized 2-terminal devices can have interesting applications: non-volatile multi-valued memories and two-element oscillators such as the Duffing oscillator, the forced Josephson junction circuit, and the Mathieu equation.

2 Non-Volatility Property of Memristors

In this section, we study the non-volatility conditions for the four classes of memristors defined in [2].

2.1 Ideal memristors

The Memristor is a 2-terminal electronic device, which was postulated in [4, 5, 6]. An ideal memristor can be described by a constitutive relation between the charge q and the flux φ,

$$q = g(\varphi) \quad \text{or} \quad \varphi = f(q), \tag{1}$$

where $g(\cdot)$ and $f(\cdot)$ are differentiable scalar-valued functions. Its terminal voltage v and terminal current i are described by

$$i = G(\varphi)v \quad \text{or} \quad v = R(q)i, \tag{2}$$

where

$$v = \frac{d\varphi}{dt} \quad \text{and} \quad i = \frac{dq}{dt}, \tag{3}$$

which represent Faraday's law of induction and its dual law, respectively. The nonlinear functions $G(\varphi)$ and $R(\varphi)$, called memductance and memristance, respectively, are defined by

$$G(\varphi) \triangleq \frac{dg(\varphi)}{d\varphi}, \quad \text{and} \quad R(q) \triangleq \frac{df(q)}{dq}. \tag{4}$$

They represent the slope of the scalar function $q = g(\varphi)$ and $\varphi = f(q)$, respectively (called the memristor constitutive relation).

Thus, the voltage-controlled ideal memristor is defined by Eq. (1) or the state-dependent Ohm's law and its associated state equation given by

voltage-controlled ideal memristor

$$\left.\begin{array}{rcl} i & = & G(\varphi)v, \\ \dfrac{d\varphi}{dt} & = & v. \end{array}\right\} \tag{5}$$

Similarly, those for the current-controlled ideal memristor are given by

current-controlled ideal memristor

$$\left.\begin{array}{rcl} v & = & R(q)i, \\ \dfrac{dq}{dt} & = & i. \end{array}\right\} \tag{6}$$

The classification of the more generalized memristors is shown in Appendix A [2].[2]

Let us apply the voltage source $v_s(t)$ to the voltage controlled ideal memristor (5). Assume that the output of the voltage source $v_s(t)$ is set to zero for $t \geq t_0$[3], that is,

$$v_s(t) = v(t) = 0 \text{ for } t \geq t_0. \tag{7}$$

Then we obtain

$$\varphi(t) = \varphi(t_0) \quad \text{for} \quad t \geq t_0, \tag{8}$$

since the flux $\varphi(t)$ satisfies $\dfrac{d\varphi}{dt} = v = 0$ for $t \geq t_0$, Thus, if there is a real number $M > 0$ such that

$$\boxed{\mid G(\varphi(t_0)) \mid \leq M, \qquad (9)}$$

then we obtain

$$\boxed{i(t) = G(\varphi(t_0))\, v(t) = 0 \quad \text{for} \quad t \geq t_0, \qquad (10)}$$

since $v(t) = 0$ for $t \geq t_0$[4].[5] [6]

The charge $q(t)$ also holds the value $q(t_0) = g(\varphi(t_0))$ for $t \geq t_0$, since $\dfrac{dq}{dt} = i = 0$ for $t \geq t_0$, Thus the voltage-controlled ideal memristor (5) exhibits the following non-volatile state:

non-volatile state

$$\left.\begin{array}{lcl} v(t) & = & \dfrac{d\varphi(t)}{dt} = 0, \\ i(t) & = & \dfrac{q(t)}{dt} = 0, \\ \varphi(t) & = & \varphi(t_0), \\ q(t) & = & q(t_0). \end{array}\right\} (\text{ for } t \geq t_0). \tag{11}$$

That is, all state variables do not evolve for $t \geq t_0$, and the voltage-controlled ideal memristor (5) has the non-volatility property.

Similarly, if there is a real number $M > 0$ such that

$$\boxed{\mid R(q(t_0)) \mid \leq M, \qquad (12)}$$

then the current-controlled ideal memristor (6) driven by the current source $i_s(t)$ has the non-volatility property, where we set $i_s(t) = 0$ for $t \geq t_0$. Thus we conclude as follows:

---

[2] We slightly modified the definition of the extended memristor.

[3] Equivalently, we can assume that the memristor is short-circuited for $t \geq t_0$, that is, $v(t) = 0$ for $t \geq t_0$ [7]).

[4] If there exists a real number M such that $\mid G(x) \mid \leq M$ for all x, then $G(x)$ is <u>bounded</u>. If $G(x)$ is bounded, then Eq. (9) is automatically satisfied. For example, $\dfrac{1}{x^2+1}$, $\sin(x)$, or $\tanh(x)$ are bounded, however, $\tan(x)$, $\ln(x)$, and $\dfrac{1}{x}$ are unbounded.

[5] Consider the memristor defined by $i = G(\varphi)v = \dfrac{v}{\varphi}$, where $G(\varphi) = \dfrac{1}{\varphi}$. Its constitutive relation is given by $q = \ln \mid \varphi \mid$. If $\varphi(t_0) = 1$, then $\mid G(\varphi(t_0) \mid = 1$, but if $\varphi(t_0) = 0$, then $\lim\limits_{\varphi(t_0) \to 0} \mid G(\varphi(t_0) \mid \to \infty$. In this case, $\mid G(\varphi) \mid < M$ does not hold for all φ and a real number $M > 0$. Thus, we assume that $\mid G(\varphi(t_0)) \mid < M$ for certain value of $\varphi(t_0)$.

[6] $f(x)$ is <u>locally bounded</u> if for any x there exists a neighborhood A of x such that $f(A)$ is a bounded set, that is, for some $M > 0$, $f(x) \leq M$ for all $x \in A$.

If there exists a real number $M > 0$ such that $\mid G(\varphi(t_0)) \mid \leq M$ and $\mid R(q(t_0)) \mid \leq M$, then the ideal memristor has the non-volatility property:

• The voltage-controlled ideal memristor (5) driven by the voltage source $v_s(t)$ does not lose the values of the flux $\varphi(t_0)$ and the charge $q(t_0)$ when we set $v_s(t) = 0$ for $t \geq t_0$.

• The current-controlled ideal memristor (6) driven by the current source $i_s(t)$ does not lose the values of the flux $\varphi(t_0)$ and the charge $q(t_0)$ when we set $i_s(t) = 0$ for $t \geq t_0$.

The voltage-controlled ideal memristor (5) and the current-controlled ideal memristor (6) function as non-volatile memories.

The above property can be reformulated as follows from the point of view of the trajectory:

If the trajectories $(v(t),\ i(t))$ of Eqs. (5) and (6) <u>remain at the origin</u> on the $(v,\ i)$-plane for $t \geq t_0$, then the flux $\varphi(t)$ and $q(t)$ <u>remain unchanged</u> from $\varphi(t_0)$ and $q(t_0)$ for $t \geq t_0$, respectively.

2.1.1 Example of the non-volatility property

Consider the flux-controlled ideal memristor defined by

$$q = g(\varphi) = \tanh(\varphi). \tag{13}$$

Its terminal voltage v and terminal current i are described by

$$i = G(\varphi)v = \left(1 - \tanh^2(\varphi)\right) v, \tag{14}$$

where $v = \dfrac{d\varphi}{dt}$ and $G(\varphi) = 1 - \tanh^2(\varphi)$. Let us drive the voltage-controlled ideal generic memristor (13) with the voltage source $v_s(t)$ as shown in Fig. 3. Here, the voltage source $v_s(t)$ is given by

$$v_s(t) = \begin{cases} r\sin^2(\omega t) & \text{for} \quad 0 \leq t < 4\pi, \\ 0 & \text{for} \quad 4\pi \leq t \leq 8\pi, \\ -r\sin^2(\omega t) & \text{for} \quad 8\pi < t < 12\pi, \\ 0 & \text{for} \quad 12\pi \leq t, \end{cases} \tag{15}$$

where $r = 0.8$ and $\omega = 0.5$. The initial condition is given by $\varphi(0) = 0.5$. We can observe from Figs. 4 and 5 that the flux $\varphi(t)$ and the charge $q(t)$ <u>remain unchanged</u> during the period when $v_s(t) = 0$. Furthermore, the trajectory $(v(t),\ i(t))$ <u>remains at the origin</u> during the period when $v_s(t) = 0$. We can also observe that the Lissajous curve of $i(t)$ and $v_s(t)$ is pinched at the origin as shown in Figs. 4(d) and 5(c).

2.2 Ideal generic memristors

In this subsection we show that the ideal generic memristors defined in Appendix A have the same non-volatility property as the ideal memristor. Their Ohm's law and associated state equation are given by

voltage-controlled ideal generic memristor

$$\left.\begin{aligned} i &= G(x)v, \\ \frac{dx}{dt} &= \hat{g}(x,\ v). \end{aligned}\right\} \tag{16}$$

current-controlled ideal generic memristor

$$\left.\begin{aligned} v &= R(x)i, \\ \frac{dx}{dt} &= \hat{f}(x,\ i). \end{aligned}\right\} \tag{17}$$

Here, i, v, and x are the terminal current, the terminal voltage, and the state variable of the memristor, $G(\cdot)$, $R(x)$, $\hat{g}(\cdot)$, and $\hat{f}(\cdot)$ are continuous scalar-valued functions.

Let us drive the voltage-controlled ideal generic memristor (16) with the voltage source $v_s(t)$. Assume that the output of the voltage source $v_s(t)$ is set to zero for $t \geq t_0$, that is, $v_s(t) = v(t) = 0$ for $t \geq t_0$. Furthermore, we assume that $\hat{g}(x,\ v)$ satisfies the following condition [1]

no state change after $v = 0$

$$\hat{g}(x,\ 0) = 0 \ \text{ for all } \ x. \tag{18}$$

Then the state equation is given by

$$\frac{dx}{dt} = \hat{g}(x,\ 0) = 0 \ \text{ for } \ t \geq t_0. \tag{19}$$

Thus, $x(t)$ satisfies $x(t) = x(t_0)$ for $t \geq t_0$. Furthermore, if there is a real number $M > 0$ such that

$$\mid G(x(t_0)) \mid \leq M, \tag{20}$$

then we obtain

$$i(t) = G(x(t_0))v(t) = 0 \ \text{ for } \ t \geq t_0, \tag{21}$$

where $v(t) = 0$ for $t \geq t_0$. Thus, if the voltage-controlled ideal generic memristor (17) satisfies Eqs. (18) and (20), then we obtain the following non-volatile state:

non-volatile state

$$x(t) = x(t_0) \ \text{ and } \ v(t) = i(t) = 0 \ \text{ for } \ t \geq t_0. \tag{22}$$

Similarly, if the current-controlled ideal generic memristor (17) driven by the current source $i_s(t)$ satisfies the following conditions[7] [1]

no state change after $i = 0$

$$f(x,\ 0) = 0 \ \text{ for all } \ x, \tag{23}$$

and if there is a real number $M > 0$ such that

$$\mid R(x(t_0)) \mid \leq M, \tag{24}$$

[7] If $\mid R(x) \mid < \infty$ for all x, then Eq. (24) is automatically satisfied.

then they also have the non-volatility property, where the current source $i_s(t)$ is set to zero for $t \geq t_0$, that is, $i_s(t) = i(t) = 0$ for $t \geq t_0$. Thus, we obtain

non-volatility property

- If the voltage-controlled memristors (16) satisfy Eqs. (18) and (20), then they have the same non-volatility property as the ideal memristor.
- If the current-controlled memristors (17) satisfy Eqs. (23) and (24), then they have the same non-volatility property as the ideal memristor.

2.3 Generic and extended memristors

In this subsection, we show that the generic and extended memristors defined in Appendix A have the same non-volatility as the ideal memristor, if the additional condition is satisfied. Their Ohm's law and associated state equation are given by

voltage-controlled generic memristor

$$\left.\begin{aligned} i &= \tilde{G}(\boldsymbol{x})v, \\ \frac{d\boldsymbol{x}}{dt} &= \tilde{\boldsymbol{g}}(\boldsymbol{x},\ v). \end{aligned}\right\} \tag{25}$$

current-controlled generic memristor

$$\left.\begin{aligned} v &= \tilde{R}(\boldsymbol{x})i, \\ \frac{d\boldsymbol{x}}{dt} &= \tilde{\boldsymbol{f}}(\boldsymbol{x},\ i). \end{aligned}\right\} \tag{26}$$

voltage-controlled extended memristor

$$\left.\begin{aligned} i &= \hat{G}(\boldsymbol{x},\ v)v, \\ \frac{d\boldsymbol{x}}{dt} &= \tilde{\boldsymbol{g}}(\boldsymbol{x},\ v). \end{aligned}\right\} \tag{27}$$

current-controlled extended memristor

$$\left.\begin{aligned} v &= \hat{R}(\boldsymbol{x},\ i)i, \\ \frac{d\boldsymbol{x}}{dt} &= \tilde{\boldsymbol{f}}(\boldsymbol{x},\ i). \end{aligned}\right\} \tag{28}$$

Here, i, v, and $\boldsymbol{x} = (x_1,\ x_2,\ \cdots,\ x_n) \in \mathbb{R}^n$ indicate the terminal current, the terminal voltage, and the state variables of the memristor, respectively, $\tilde{G}(\cdot)$, $\hat{G}(\cdot)$, $\tilde{R}(\cdot)$, and $\hat{R}(\cdot)$ are continuous scalar-valued functions, $\tilde{\boldsymbol{g}} = (\tilde{g}_1,\ \tilde{g}_2,\ \cdots,\ \tilde{g}_n) : \mathbb{R}^n \to \mathbb{R}^n$, and $\tilde{\boldsymbol{f}} = (\tilde{f}_1,\ \tilde{f}_2,\ \cdots,\ \tilde{f}_n) : \mathbb{R}^n \to \mathbb{R}^n$.

Assume that the voltage-controlled memristors (25) and (27) are driven by the voltage source $v_s(t)$ and assume that $\tilde{\boldsymbol{g}}(\boldsymbol{x},\ v)$ satisfies the following state conservation condition [1]

no state change after $v = 0$

$$\tilde{\boldsymbol{g}}(\boldsymbol{x},\ 0) = \boldsymbol{0} \quad \text{for all} \quad \boldsymbol{x}. \tag{29}$$

where $\boldsymbol{0}$ denotes a zero vector whose components are all 0, i.e., $\boldsymbol{0} = (0,\ 0, \cdots,\ 0)$.

Assume next that the output of the voltage source is set to zero for $t \geq t_0$, that is, $v_s(t) = v(t) = 0$ for $t \geq t_0$. Then we get

$$\frac{d\boldsymbol{x}}{dt} = \tilde{\boldsymbol{g}}(\boldsymbol{x},\ v) = 0, \quad \text{for} \quad t \geq t_0, \tag{30}$$

and therefore

$$\boldsymbol{x}(t) = \boldsymbol{x}(t_0) \quad \text{for} \quad t \geq t_0, \tag{31}$$

Furthermore, if there is a real number $M > 0$ such that

$$| \tilde{G}(\boldsymbol{x}(t_0)) | \leq M \quad \text{and} \quad | \hat{G}(\boldsymbol{x}(t_0),\ 0) \leq M, \tag{32}$$

then we obtain

$$i(t) = \tilde{G}\big(\boldsymbol{x}(t_0)\big)v(t) = 0 \ \text{ and } i(t) = \hat{G}\big(\boldsymbol{x}(t_0),\ v(t)\big)v(t) = 0, \tag{33}$$

for $t \geq t_0$, where $v_s(t) = v(t) = 0$ for $t \geq t_0$[8]. Thus, if the voltage-controlled memristors (25) and (27) satisfy Eqs. (29) and (32), then we obtain the following non-volatile state:

non-volatile state

$$\boldsymbol{x}(t) = \boldsymbol{x}(t_0) \ \text{ and } \ v(t) = i(t) = 0 \ \text{ for } \ t \geq t_0. \tag{34}$$

Similarly, if the current-controlled memristors (26) and (28) driven by the current source $i_s(t)$ satisfy the following condition [1]

no state change after $i = 0$

$$\tilde{\boldsymbol{f}}(\boldsymbol{x},\ 0) = \boldsymbol{0} \ \text{ for all } \ \boldsymbol{x}, \tag{35}$$

then they also have the non-volatility property. Here we have assumed that there is a real number $M > 0$ such that [9]

$$| \tilde{R}(\boldsymbol{x}(t_0)) | \leq M \quad \text{and} \quad | \hat{R}(\boldsymbol{x}(t_0),\ 0) | \leq M, \tag{36}$$

and we set the output of the current source is set to zero for $t \geq t_0$, that is, $i_s(t) = i(t) = 0$ for $t \geq t_0$.

- If the voltage-controlled memristors (25) and (27) satisfy Eqs. (29) and (32), then they have the same non-volatility property as the ideal memristor.
- If the current-controlled memristors (26) and (28) satisfy Eqs. (35) and (36), then they have the same non-volatility property as the ideal memristor.

[8] If if there is a real number $M > 0$ such that $| \tilde{G}(\boldsymbol{x}) | \leq M$ and $| \hat{G}(\boldsymbol{x},\ 0) | < M$ for all $\boldsymbol{x}$, then Eq. (32) are automatically satisfied.

[9] If there is a real number $M > 0$ such that $| \tilde{R}(\boldsymbol{x}) | \leq M$ and $| \hat{R}(\boldsymbol{x},\ 0) | < M$ for all $\boldsymbol{x}$, then Eq. (36) are automatically satisfied.

3 Non-volatility Conditions for 2-terminal Devices

In this section, we show the 2-terminal devices, which do not belong to the above four classes of memristors, but have the same non-volatile property as the ideal memristor.

3.1 2-terminal devices

Consider the voltage-controlled 2-terminal device defined by

voltage-controlled 2-terminal device

$$\left.\begin{array}{lcl} i & = & W(\varphi,\ v), \\ \dfrac{d\varphi}{dt} & = & v, \end{array}\right\} \tag{37}$$

or equivalently

voltage-controlled 2-terminal device

$$\frac{dq}{dt} = W\left(\varphi,\ \frac{d\varphi}{dt}\right), \tag{38}$$

where i, v, q and φ are the terminal current, the terminal voltage, the charge, and the flux, respectively, and $W(\varphi,\ v)$ is a scalar-valued function.

Let us drive the voltage-controlled 2-terminal device (37) by the voltage source $v_s(t)$, where we set $v_s(t) = 0$ for $t \geq t_0$. Then, we get

$$\frac{d\varphi}{dt} = v = 0, \tag{39}$$

and

$$\varphi(t) = \varphi(t_0), \quad \text{for} \quad t \geq t_0, \tag{40}$$

where $v_s(t) = v(t)$ for $t \geq t_0$. Assume that voltage-controlled 2-terminal device (37) satisfies the following condition[10]

non-volatility condition

$$W(\varphi(t_0),\ v) = 0 \quad \text{for} \quad v = 0. \tag{41}$$

Then, we obtain

$$i(t) = \frac{dq(t)}{dt} = W(\varphi(t_0),\ 0) = 0 \quad \text{for} \quad t \geq t_0. \tag{42}$$

if we substitute

$$v(t) = \frac{d\varphi(t)}{dt} = 0, \tag{43}$$

into Eqs. (37). Thus, we obtain the following non-volatile state:

$$\text{If} \quad v_s(t) = 0 \quad \text{for} \quad t \geq t_0, \text{ then } \ v(t) = i(t) = 0,\ \varphi(t) = \varphi(t_0), \text{ and } q(t) = q(t_0) \quad \text{for} \quad t \geq t_0. \tag{44}$$

[10] If $W(\varphi,\ 0) = 0$ for all φ, then Eq. (41) is automatically satisfied. Note that we cannot always factor φ out of $W(\varphi,\ v)$. That is, $W(\varphi,\ v)$, which satisfies $W(\varphi,\ 0) = 0$, does not always have the form $G(\varphi)v$, where $G(\varphi)$ is a scaler-valued function. For example, if $W(\varphi,\ v) = \dfrac{v + 0.5(\mid v-1 \mid - \mid v+1 \mid)}{\varphi}$, then $W(\varphi(t_0),\ 0) = 0$ except for $\varphi(t_0) = 0$. However, we cannot factor φ out of $W(\varphi,\ v)$.

That is, the 2-terminal device (37) has the same non-volatility property as the ideal memristor (5):

> The 2-terminal device (37) driven by the voltage source $v_s(t)$ has the same non-volatility property as the ideal memristor.
>
> That is, the device (37) does not lose the values of the flux $\varphi(t_0)$ and the charge $q(t_0)$ when we set $v_s(t) = 0$ for $t \geq t_0$ and we assume that $W(\varphi(t_0),\ 0) = 0$.

Similarly, consider the 2-terminal device defined by

current-controlled 2-terminal device

$$\left.\begin{array}{rcl} v & = & Z(q,\ i), \\ \dfrac{dq}{dt} & = & i, \end{array}\right\} \qquad (45)$$

Assume that $Z(q,\ v)$ satisfies the following non-volatility condition

non-volatility condition

$$Z(q(t_0),\ v) = 0 \ \text{ for } \ v = 0. \qquad (46)$$

Then the 2-terminal device (45) has the non-volatility property. However, the 2-terminal devices (37) and (45) cannot be described by a constitutive relation between the charge q and the flux φ.

> The 2-terminal devices defined by Eqs. (37) and (45) can have the same non-volatility property as the ideal memristor, but do not belong to the four classes of memristors, which are defined in Appendix A. For this reason, we use the term "2-terminal devices" instead of "memristors" or "memristive systems".

3.2 Generalized 2-terminal devices

In this section, we generalize the 2-terminal device defined in Sec. 3.1. It has the same non-volatility property as the ideal memristor, which can be described as follows:

- generalized voltage-controlled 2-terminal device

$$\left.\begin{array}{rcl} i & = & W(\boldsymbol{x},\ v), \\ \dfrac{d\boldsymbol{x}}{dt} & = & \tilde{\boldsymbol{g}}(\boldsymbol{x},\ v). \end{array}\right\} \qquad (47)$$

- generalized current-controlled 2-terminal device

$$\left.\begin{array}{rcl} v & = & Z(\boldsymbol{x},\ i), \\ \dfrac{d\boldsymbol{x}}{dt} & = & \tilde{\boldsymbol{f}}(\boldsymbol{x},\ i). \end{array}\right\} \qquad (48)$$

where $\boldsymbol{x} = (x_1,\ x_2,\ \cdots,\ x_n) \in \mathbb{R}^n$, $\tilde{\boldsymbol{g}} = (\tilde{g}_1,\ \tilde{g}_2,\ \cdots,\ \tilde{g}_n) : \mathbb{R}^n \to \mathbb{R}^n$, $\tilde{\boldsymbol{f}} = (\tilde{f}_1,\ \tilde{f}_2,\ \cdots,\ \tilde{f}_n) : \mathbb{R}^n \to \mathbb{R}^n$, and $W(\boldsymbol{x},\ v)$, $Z(\boldsymbol{x},\ i)$, $\tilde{\boldsymbol{g}}(\boldsymbol{x},\ i)$, and $\tilde{\boldsymbol{f}}(\boldsymbol{x},\ i)$ are scalar-valued functions.

The generalized 2-terminal devices (47) and (48) do not belong to the four classes of memristors in Appendix A. However, they include the four classes of memristors as a special case.

Let us drive the voltage-controlled 2-terminal device (47) by the voltage source $v_s(t)$, where we set $v_s(t) = 0$ for $t \geq t_0$. Assume that

$$\tilde{\boldsymbol{g}}(\boldsymbol{x},\ 0) = \boldsymbol{0} \ \text{ for all } \ \boldsymbol{x}. \tag{49}$$

Then, we obtain

$$\boldsymbol{x}(t) = \boldsymbol{x}(t_0) \ \text{ for } \ t \geq t_0. \tag{50}$$

since $\dfrac{d\boldsymbol{x}(t)}{dt} = \tilde{\boldsymbol{g}}(\boldsymbol{x}(t),\ v(t)) = 0$, for $v_s(t) = v(t) = 0$ and $t \geq t_0$.

Assume next that[11].

$$W(\boldsymbol{x}(t_0),\ 0) = 0. \tag{51}$$

Then, we obtain

$$i(t) = W\big(\boldsymbol{x}(t),\ v(t)\big) = 0, \tag{52}$$

since $\boldsymbol{x}(t) = \boldsymbol{x}(t_0)$ and $v(t) = 0$ for $t \geq t_0$. Thus, the device (47) has the following non-volatile state:

non-volatile state

$$\boldsymbol{x}(t) = \boldsymbol{x}(t_0) \ \text{ and } \ v(t) = i(t) = 0 \ \text{ for } \ t \geq t_0. \tag{53}$$

Thus, the non-volatility condition for Eq. (47) is given by

non-volatility condition for Eq. (47)

$$\left.\begin{array}{l} W(\boldsymbol{x}(t_0),\ 0) = 0, \\ \tilde{\boldsymbol{g}}(\boldsymbol{x},\ 0) = \boldsymbol{0} \ \text{ for all } \ \boldsymbol{x}. \end{array}\right\} \tag{54}$$

Similarly, let us drive the current-controlled 2-terminal device (48) by the current source $i_s(t)$, where $i_s(t) = 0$ for $t \geq t_0$. Then, this device has the same non-volatile state if the following condition is satisfied:

non-volatility condition for Eq. (48)

$$\left.\begin{array}{l} Z(\boldsymbol{x}(t_0),\ 0) = 0, \\ \tilde{\boldsymbol{f}}(\boldsymbol{x},\ 0) = \boldsymbol{0} \ \text{ for all } \ \boldsymbol{x}. \end{array}\right\} \tag{55}$$

[11] If $W(\boldsymbol{x},\ 0) = 0$ for all $\boldsymbol{x}$, then Eq. (51) is automatically satisfied.

Our conclusion is as follows:

> The generalized voltage-controlled 2-terminal device (47) has the non-volatility property if Eq. (54) is satisfied, that is,
>
> • The voltage-controlled generalized 2-terminal device (47) driven by the voltage source $v_s(t)$ does not lose the values of $\boldsymbol{x}(t_0)$ when we set $v_s(t) = 0$ for $t \geq t_0$.

> The generalized current-controlled 2-terminal device (48) has the non-volatility property if Eq. (55) is satisfied, that is,
>
> • The current-controlled generalized 2-terminal device (48) driven by the current source $i_s(t)$ does not lose the values of $\boldsymbol{x}(t_0)$ when we set $i_s(t) = 0$ for $t \geq t_0$.

4 Pinched Hysteresis Loops

As shown in Sec. 2.1, the Lissajous curve of $i(t)$ and $v_s(t)$ is pinched at the origin. In this section, we observe the pinched hysteresis loops of the four classes of memristors and the 2-terminal devices by applying a sinusoidal voltage source.

- **Example 1. flux-controlled ideal memristor**
  Consider the flux-controlled ideal memristor defined by

  flux-controlled ideal memristor

  $$q = g(\varphi) = \tanh(\varphi). \tag{56}$$

  Its terminal voltage v and terminal current i are given by

  state-dependent Ohm's law

  $$i = G(\varphi)v = \left(1 - \tanh^2(\varphi)\right) v = \operatorname{sech}^2(\varphi)\, v, \tag{57}$$

  where $G(\varphi) \triangleq 1 - \tanh^2(\varphi) = \operatorname{sech}^2(\varphi)$, and Faraday's law is is given by

  $$v = \frac{d\varphi}{dt} \tag{58}$$

  Let us apply a sinusoidal voltage source $v_s(t) = r\sin(\omega t)$ for $t \geq 0$. The initial condition is given by $\varphi(0) = 0$. By plotting the Lissajous curve of $i(t)$ and $v(t)$, we obtain the pinched hysteresis loops shown in Fig. 6(a)-(h). The Lissajous curve shown in Fig. 6(f) is similar to the pinched hysteresis loop shown in [8]. We conclude as follows:

  > Since the function $G(\varphi)$ is bounded, the current $i(t) = G(\varphi(t))\, v(t) = 0$ when $v(t) = 0$. This means that the Lissajous curve of $i(t)$ and $v(t)$ passes through the origin and is pinched at the origin as shown in Fig. 6(a)-(h).

The flux-controlled ideal memristor (56) has the non-volatility property, that is, $\varphi(t)$ and $q(t)$ do not change during the period when $v(t) = 0$, as shown in the example of Sec. 2.1.1.

- **Example 2. flux-controlled ideal memristor**
  Consider the flux-controlled ideal memristor defined by

flux-controlled ideal memristor

$$q = g(\varphi) = \tanh(\varphi) + d\varphi, \tag{59}$$

where $d > 0$ is the parameter. Its terminal voltage v and terminal current i are given by

state-dependent Ohm's law

$$i = G(\varphi)v = \left(1 + d - \tanh^2(\varphi)\right) v = (\mathrm{sech}^2(\varphi) + d)\, v, \tag{60}$$

where $G(\varphi) \triangleq \mathrm{sech}^2(\varphi) + d$, and Faraday's law is is given by

$$v = \frac{d\varphi}{dt} \tag{61}$$

Let us apply a sinusoidal voltage source $v_s(t) = r\sin(\omega t)$ for $t \geq 0$. The initial condition is given by $\varphi(0) = 0$. By plotting the Lissajous curve of $i(t)$ and $v(t)$, we obtain the pinched hysteresis loops shown in Fig. 6(i)-(j). The Lissajous curve shown in Fig. 6(i) is very similar to the pinched hysteresis loops shown in [8]. We conclude as follows:

Since the function $G(\varphi)$ is bounded, the current $i(t) = G(\varphi(t))\, v(t) = 0$ when $v(t) = 0$. This means that the Lissajous curve of $i(t)$ and $v(t)$ passes through the origin and is pinched at the origin as shown in Fig. 6(i)-(j).

The flux-controlled ideal memristor (59) has the non-volatility property, that is, $\varphi(t)$ and $q(t)$ do not change during the period when $v(t) = 0$. This is because $\dfrac{d\varphi}{dt} = 0$ for this period and $q(t)$ satisfies the constitutive relation $q(t) = g(\varphi(t))$.

- **Example 3. voltage-controlled extended memristor**
  Consider next the voltage-controlled extended memristor defined by

voltage-controlled extended memristor

$$\left.\begin{aligned} i &= G(\varphi,\, v)v = \left\{\left(1 - \tanh^2(\varphi)\right) e^{av}\right\} v, \\ \frac{d\varphi}{dt} &= v, \end{aligned}\right\} \tag{62}$$

where a is the parameter and $G(\varphi,\, v) \triangleq \big(1-\tanh^2(\varphi)\big)\, e^{av}$.

Let us apply a sinusoidal voltage source $v_s(t) = r\sin(\omega t)$ for $t \geq 0$. The initial condition is given by $\varphi(0) = 0$. By plotting the Lissajous curve of $i(t)$ and $v(t)$, we obtain the pinched hysteresis loops shown in Fig. 6(k)-(l). We conclude as follows:

> Since the function $G(\varphi,\, 0) = 1-\tanh^2(\varphi)$ is bounded, the current $i(t) = G(\varphi(t))\, v(t) = 0$ when $v(t) = 0$. This means that the Lissajous curve of $i(t)$ and $v(t)$ passes through the origin and is pinched at the origin as shown in Fig. 6(k)-(l).

> The voltage-controlled extended memristor (62) has the non-volatility property, that is, $\varphi(t)$ does not change during the period when $v(t) = 0$, since $\dfrac{d\varphi}{dt} = 0$ for this period.

- **Example 4. voltage-controlled extended memristor**
  Consider next the voltage-controlled extended memristor defined by

> voltage-controlled extended memristor
>
> $$\left.\begin{aligned} i &= G(\varphi,\, v)v = \big\{\big(1-\tanh^2(\varphi)\big)\, u(v+b)\big\}\, v, \\ \frac{d\varphi}{dt} &= v, \end{aligned}\right\} \qquad (63)$$

where b is the parameter, $u(v)$ is the unit step function[12], which is equal to 0 for $v < 0$ and 1 for $v \geq 0$, and $G(\varphi,\, v) \triangleq \big(1-\tanh^2(\varphi)\big)\, u(v+b)$ is bounded.

Let us apply a sinusoidal voltage source $v_s(t) = r\sin(\omega t)$ for $t \geq 0$. The initial condition is given by $\varphi(0) = 0$. By plotting the Lissajous curve of $i(t)$ and $v(t)$, we obtain the pinched hysteresis loops shown in Fig. 7(m)-(o). We conclude as follows:

> Since $G(\varphi,\, v)$ is bounded, the current $i(t) = G\big(\varphi(t),\, v(t)\big)\, v(t) = 0$ when $v(t) = 0$. This means that the Lissajous curve of $i(t)$ and $v(t)$ passes through the origin and is pinched at the origin as shown in Fig. 7(m)-(o).

> The voltage-controlled extended memristor (62) has the non-volatility property, that is, $\varphi(t)$ does not change during the period when $v(t) = 0$, since $\dfrac{d\varphi}{dt} = 0$ for this period.

- **Example 5. voltage-controlled 2-terminal device**
  Consider the voltage-controlled 2-terminal device defined by

[12] A smooth approximation of the unit step function $u(v)$ is given by the function $\dfrac{1+\tanh(kv)}{2} = \dfrac{1}{1+e^{-2kv}}$ for $k \gg 1$, which can be practically used in place of $u(v)$.

voltage-controlled 2-terminal device

$$\left.\begin{array}{rcl} i & = & W(\varphi,\ v) = H(k(\varphi,\ v)), \\ \dfrac{d\varphi}{dt} & = & v, \end{array}\right\} \tag{64}$$

where

$$\left.\begin{array}{rcl} H(s) & \triangleq & 0.5(\mid s+1 \mid - \mid s-1 \mid), \\ k(\varphi,\ v) & \triangleq & \left(1-\tanh^2(\varphi)\right) v. \end{array}\right\} \tag{65}$$

The function $W(\varphi,\ v)$ satisfies

$$W(\varphi,\ v) = H(k(\varphi,\ v)) = 0 \ \text{ for } \ v = 0, \tag{66}$$

since $k(\varphi,\ 0) = 0$ and $H(0) = 0$.

Let us apply a sinusoidal voltage source $v_s(t) = r\sin(\omega t)$ for $t \geq 0$. The initial condition is given by $\varphi(0) = 0$. By plotting the Lissajous curve of $i(t)$ and $v(t)$, we obtain the pinched hysteresis loops shown in Fig. 7(p)-(s). The Lissajous curve shown in Fig. 7(p) is very similar to the experimentally measured pinched hysteresis loop shown in [9]. We conclude as follows:

Since $W(\varphi,\ 0) = 0$, the current $i(t) = W\big(\varphi(t),\ v(t)\big) = 0$ when $v(t) = 0$. This means that the Lissajous curve of $i(t)$ and $v(t)$ passes through the origin and is pinched at the origin as shown in Fig. 7(p)-(s).

The voltage-controlled 2-terminal device (64) has the non-volatility property, that is, $\varphi(t)$ does not change during the period when $v(t) = 0$, since $\dfrac{d\varphi}{dt} = 0$ for this period.

- **Example 6. voltage-controlled 2-terminal device**
  Consider the voltage-controlled 2-terminal device defined by

voltage-controlled 2-terminal device

$$\left.\begin{array}{rcl} i & = & W(\varphi,\ v) = H(k(\varphi,\ v)), \\ \dfrac{d\varphi}{dt} & = & v. \end{array}\right\} \tag{67}$$

Here $H(s)$ and $k(\varphi,\ v)$ is defined by

$$\left.\begin{array}{rcl} H(s) & \triangleq & \tanh(cs), \\ k(\varphi,\ v) & \triangleq & \left(1-\tanh^2(\varphi)\right) v, \end{array}\right\} \tag{68}$$

where c is a constant. The function $W(\varphi,\ v)$ satisfies

$$W(\varphi,\ v) = H(k(\varphi,\ v)) = 0 \ \text{ for } \ v = 0, \tag{69}$$

since $k(\varphi,\ 0) = 0$ and $H(0) = 0$.

Let us apply a sinusoidal voltage source $v_s(t) = r\sin(\omega t)$ for $t \geq 0$. The initial condition is given by $\varphi(0) = 0$. By plotting the Lissajous curve of $i(t)$ and $v(t)$, we obtain the pinched hysteresis loops shown in Fig. 7(t)-(u). We conclude as follows:

Since $W(\varphi,\ 0) = 0$, the current $i(t) = W\big(\varphi(t),\ v(t)\big) = 0$ when $v(t) = 0$. This means that the Lissajous curve of $i(t)$ and $v(t)$ passes through the origin and is pinched at the origin as shown in Fig. 7(t)-(u).

The voltage-controlled 2-terminal device (67) has the non-volatility property, that is, $\varphi(t)$ does not change during the period when $v(t) = 0$, since $\dfrac{d\varphi}{dt} = 0$ for this period.

- **Example 7. voltage-controlled 2-terminal device**
  Consider next the voltage-controlled 2-terminal device defined by

voltage-controlled 2-terminal device

$$\left.\begin{array}{l} i = W(\varphi,\, v), \\ \dfrac{d\varphi}{dt} = v. \end{array}\right\} \tag{70}$$

Here we consider the case where $W(\varphi,\, v)$ is defined by

$$\left.\begin{array}{rcl} W_1(\varphi,\, v) & = & \left(1 - \tanh^2(\varphi)\right) v, \\ W_2(\varphi,\, v) & = & -\left(1 - \tanh^2(\varphi)\right) v, \\ W_3(\varphi,\, v) & = & \mathrm{sign}(v)\left(1 - \tanh^2(\varphi)\right) v, \\ W_4(\varphi,\, v) & = & -\mathrm{sign}(v)\left(1 - \tanh^2(\varphi)\right) v, \\ W_5(\varphi,\, v) & = & u(v)\left(1 - \tanh^2(\varphi)\right) v, \\ W_6(\varphi,\, v) & = & -u(-v)\left(1 - \tanh^2(\varphi)\right) v, \\ W_7(\varphi,\, v) & = & u(-v)\left(1 - \tanh^2(\varphi)\right) v, \\ W_8(\varphi,\, v) & = & -u(v)\left(1 - \tanh^2(\varphi)\right) v, \\ W_9(\varphi,\, v) & = & H\left(\mid v \mid \left(1 - \tanh^2(\varphi)\right)\right), \\ W_{10}(\varphi,\, v) & = & \left(1 - \tanh^2(\varphi)\right) e^v v, \\ W_{11}(\varphi,\, v) & = & \ln \mid W_1(\varphi,\, v) \mid . \end{array}\right\} \tag{71}$$

where the sign function: $\mathrm{sgn}(v)$ is defined by [13]

$$\mathrm{sgn}(v) = \left\{\begin{array}{lll} -1 & for & v < 0, \\ 0 & for & v = 0, \\ 1 & for & v > 0. \end{array}\right. \tag{72}$$

and

$$H(s) = 0.5\ \big(\mid s + 1 \mid - \mid s - 1 \mid\big). \tag{73}$$

The function $W_{11}(\varphi,\, v)$ is not bounded for $v = 0$. In this case, the 2-terminal device (70) does not satisfy the non-volatility condition.

[13] A smooth approximation of $\mathrm{sgn}(v)$ is given by the function $\tanh(kv)$ for $k \gg 1$, which can be practically used in place of $\mathrm{sgn}(v)$.

Let us apply a sinusoidal voltage source $v_s(t) = r\sin(\omega t)$ for $t \geq 0$. The initial condition is given by $\varphi(0) = 0$. By plotting the Lissajous curve of $i(t)$ and $v(t)$, we obtain the pinched hysteresis loops shown in Fig. 8. We conclude as follows:

> Since the function $W_i(\varphi,\, 0)$ $(i = 1,\ 2, \cdots,\ 10)$ are equal to zero, the current $i(t) = W_i\big(\varphi(t),\, v(t)\big) = 0$ when $v(t) = 0$. This means that the Lissajous curve of $i(t)$ and $v(t)$ passes through the origin and is pinched at the origin as shown Fig. 8(a)-(j).

> The voltage-controlled 2-terminal device (70) for $W_i(\varphi,\, 0)$ $(i = 1,\ 2, \cdots,\ 10)$ has the non-volatility property, that is, $\varphi(t)$ does not change during the period when $v(t) = 0$, since $\dfrac{d\varphi}{dt} = 0$ for this period.

- **Example 8. voltage-controlled extended memristor**
  Consider next the voltage-controlled extended memristor defined by

> voltage-controlled extended memristor
>
> $$\left.\begin{aligned} i &= G(\varphi,\, v)\ v \\ \frac{d\varphi}{dt} &= v, \end{aligned}\right\} \tag{74}$$

Here we consider the case where $G(\varphi,\, v)$ is defined by

$$\left.\begin{aligned}
G_1(\varphi,\, v) &= u(\varphi - 1), \\
G_2(\varphi,\, v) &= 1 - u(\varphi - 1), \\
G_3(\varphi,\, v) &= u(\varphi - 1)\ u(v + 1.5), \\
G_4(\varphi,\, v) &= u(\varphi - 1) + 0.1,, \\
G_5(\varphi,\, v) &= 1.1 - u(\varphi - 1), \\
G_6(\varphi,\, v) &= \{u(\varphi - 1)\ u(v + 1.5) + 0.1\}, \\
G_7(\varphi,\, v) &= \{u(\varphi - 1) + 0.1\}\ e^{0.2v}, \\
G_8(\varphi,\, v) &= (1.1 - u(\varphi - 1))\ e^{0.2v}, \\
G_9(\varphi,\, v) &= \{u(\varphi - 1)\ u(v + 1.5) + 0.1\}\ e^{0.2v}.
\end{aligned}\right\} \tag{75}$$

Let us apply a sinusoidal voltage source $v_s(t) = r\sin(\omega t)$ for $t \geq 0$. The initial condition is given by $\varphi(0) = 0$. By plotting the Lissajous curve of $i(t)$ and $v(t)$, we obtain the pinched hysteresis loops shown in Fig. 9. Observe the difference in the two turning points of the Lissajous curves. The Lissajous curve shown in Fig. 9(c) is similar to the pinched hysteresis loop shown in [14]. Furthermore, the Lissajous curve shown in Fig. 9(i) is similar to the pinched hysteresis loop (shoelace plot) shown in [2]. We conclude as follows:

> Since all $G_i(\varphi,\, 0)$ is bounded, the current $i(t) = G_i\big(\varphi(t),\, v(t)\big)\, v(t) = 0$ when $v(t) = 0$. This means that the Lissajous curve of $i(t)$ and $v(t)$ passes through the origin and is pinched at the origin as shown in Fig. 9.

The voltage-controlled extended memristor (74) has the non-volatility property, that is, $\varphi(t)$ does not change during the period when $v(t) = 0$, since $\dfrac{d\varphi}{dt} = 0$ for this period.

- **Example 9. voltage-controlled 2-terminal device**
  Consider the voltage-controlled extended memristor defined by Consider the voltage-controlled 2-terminal device defined by

voltage-controlled 2-terminal device

$$\left.\begin{array}{rcl} i & = & W(\varphi,\ v) = u(v+d)\ u(\varphi-1)\ h(v), \\ \dfrac{d\varphi}{dt} & = & v, \end{array}\right\} \tag{76}$$

where the scalar function $h(v)$ is defined by

$$h(v) \triangleq v - 0.5(\mid v+1 \mid - \mid v-1 \mid). \tag{77}$$

The function $W(\varphi,\ v)$ satisfies

$$W(\varphi,\ v) = u(v+d)\ u(\varphi-1)\ h(v) = 0 \quad \text{for} \quad v = 0, \tag{78}$$

where $u(s)$ is bounded and $h(v) = 0$ for $v = 0$.

Let us apply a sinusoidal voltage source $v_s(t) = r\sin(\omega t)$ for $t \geq 0$. The initial condition is given by $\varphi(0) = 0$. By plotting the Lissajous curve of $i(t)$ and $v(t)$, we obtain the pinched hysteresis loops shown in Fig. 10. Observe that as the parameter d increases, the newly created triangle becomes larger. These Lissajous curves are very similar to the experimentally measured pinched hysteresis loops shown in [10]. We conclude as follows:

Since $W(\varphi,\ 0) = 0$, the current $i(t) = W\big(\varphi(t),\ v(t)\big) = 0$ when $v(t) = 0$. This means that the Lissajous curve of $i(t)$ and $v(t)$ passes through the origin and is pinched at the origin as shown in Fig. 10.

The voltage-controlled 2-terminal device (76) has the non-volatility property, that is, $\varphi(t)$ does not change during the period when $v(t) = 0$, since $\dfrac{d\varphi}{dt} = 0$ for this period.

- **Example 10. voltage-controlled 2-terminal device**
  Consider the voltage-controlled extended memristor defined by Consider the voltage-controlled 2-terminal device defined by

voltage-controlled 2-terminal device

$$\left.\begin{array}{rcl} i & = & W(\varphi,\ v) \\ \dfrac{d\varphi}{dt} & = & v, \end{array}\right\} \tag{79}$$

Assume that the function $W(\varphi,\ v)$ is given by

$$\left.\begin{array}{rcl} W_1(\varphi,\, v) & = & u(\varphi-1)\ u(v)\ v, \\ W_2(\varphi,\, v) & = & u(\varphi-1)\ u(v)\ u(0.8-v)\ v, \\ W_3(\varphi,\, v) & = & h_1\big(W_1(\varphi,\, v)\big), \\ W_4(\varphi,\, v) & = & h_2\big(W_2(\varphi,\, v)\big), \end{array}\right\} \tag{80}$$

where the scalar function $h_i(\cdot)$ $(i=1,\ 2)$ is defined by

$$\left.\begin{array}{rcl} h_1(s) & \triangleq & v-0.5(\mid s+0.8\mid-\mid s-0.8\mid), \\ h_2(s) & \triangleq & v-0.5(\mid s+0.5\mid-\mid s-0.5\mid). \end{array}\right\} \tag{81}$$

The functions $W(\varphi,\ v)_i$ $(i=1,\ 2)$ satisfy

$$W_i(\varphi,\ v)=0 \ \text{ for } \ v=0, \tag{82}$$

since $u(\varphi-1)$ is bounded, and $u(0)=0$ and $h(0)=0$. Thus, we obtain the following non-volatility property:

Let us apply a sinusoidal voltage source $v_s(t)=r\sin(\omega t)$ for $t\geq 0$. The initial condition is given by $\varphi(0)=0$. By plotting the Lissajous curve of $i(t)$ and $v(t)$, we obtain the pinched hysteresis loops shown in Fig. 11. Note that the Lissajous curve in the third quadrant is squashed into a line segment. The Lissajous curve shown in Fig. 11(a) is similar to the pinched hysteresis loops shown in [8]. Furthermore, the Lissajous curve shown in Fig. 11(e) is very similar to the experimentally measured pinched hysteresis loops shown in [10]. We conclude as follows:

> Since $W_i(\varphi,\ 0)=0$, the current $i(t)=W_i\big(\varphi(t),\ v(t)\big)=0$ when $v(t)=0$. This means that the Lissajous curve of $i(t)$ and $v(t)$ passes through the origin and is pinched at the origin shown in Fig. 11.

> The voltage-controlled 2-terminal device (79) has the non-volatility property, that is, $\varphi(t)$ does not change during the period when $v(t)=0$, since $\dfrac{d\varphi}{dt}=0$ for this period.

- **Example 11. voltage-controlled extended memristor**
  Consider the voltage-controlled extended memristor defined by

> voltage-controlled extended memristor
>
> $$\left.\begin{array}{l} i=G(\varphi,\, v)\ v, \\ \dfrac{d\varphi}{dt}=v, \end{array}\right\} \tag{83}$$

where

$$G(\varphi,\, v)\triangleq u(v)\ \big\{u(0.95-\varphi)+0.1\big\}+u(-v)\ \big\{u(1.3-\varphi)+0.1\big\}. \tag{84}$$

Since the unit step function $u(\cdot)$ is bounded, $G(\varphi,\, 0)$ is bounded.

Let us apply a sinusoidal voltage source $v_s(t)=r\sin(\omega t)$ for $t\geq 0$. The initial condition is given by $\varphi(0)=0.8$ and the parameters are given by $r=0.1$ and $\omega=0.3$. By plotting the Lissajous curve of $i(t)$ and $v(t)$, we obtain the pinched hysteresis loops shown in Fig. 12. The Lissajous curve in Fig. 12(b) is plotted on a semi-log graph. These Lissajous curves are very similar to the experimentally measured Lissajous curves shown in [11]. We conclude as follows:

Since $G(\varphi,\ 0)$ is bounded, the current $i(t) = G\big(\varphi(t),\, v(t)\big)\, v(t) = 0$ when $v(t) = 0$. This means that the Lissajous curve of $i(t)$ and $v(t)$ on a linear-scale graph passes through the origin and is pinched at the origin as shown in Fig. 12(a).

The voltage-controlled extended memristor (83) has the non-volatility property, that is, $\varphi(t)$ does not change during the period when $v(t) = 0$, since $\dfrac{d\varphi}{dt} = 0$ for this period.

- **Example 12. voltage-controlled 2-terminal device**
  Consider the voltage-controlled 2-terminal device defined by

voltage-controlled 2-terminal device

$$\left.\begin{array}{rcl} i & = & W(\varphi,\ v) = H\big(k(\varphi,\ v)\big), \\ \dfrac{d\varphi}{dt} & = & v, \end{array}\right\} \tag{85}$$

where

$$\left.\begin{array}{rcl} H(s) & \triangleq & 0.5\big(\mid s+0.8 \mid - \mid s-0.8 \mid\big), \\ k(\varphi,\ v) & \triangleq & u(1-\varphi)\ v. \end{array}\right\} \tag{86}$$

The function $W(\varphi,\ v)$ satisfies

$$W(\varphi,\ v) = H\big(k(\varphi,\ v)\big) = 0 \ \text{ for } \ v = 0, \tag{87}$$

since $k(\varphi,\ 0) = 0$ and $H(0) = 0$.

Let us apply a sinusoidal voltage source $v_s(t) = r\sin(\omega t)$ for $t \geq 0$. The initial condition is given by $\varphi(0) = 0.8$. By plotting the Lissajous curve of $i(t)$ and $v(t)$, we obtain the pinched hysteresis loops shown in Fig. 13. The Lissajous curves shown in Fig. 13(a) are very similar to the experimentally measured pinched hysteresis loop (plotted on a linear-scale graph) shown in [12]. Note that the Lissajous curve in Fig. 13(b) is plotted on a semi-log graph.

The Lissajous curve on the semi-log graph does not remain in a bounded region, since $i(t) = 0$ when $v(t) = 0$ (see Fig. 13(b)). Thus, we added the signal $e(t)$ to the current $i(t)$, that is,

$$\left.\begin{array}{rcl} i_e(t) & = & i(t) + e(t) = H\Big(k\big(\varphi(t),\ v(t)\big)\Big) + e(t), \\ e(t) & = & \mathrm{sign}\big(\cos(\omega t)\big) + 1.5, \end{array}\right\} \tag{88}$$

where $v(t) = v_s(t) = r\sin(\omega t)$. Then, the Lissajous curve of $\ln(\mid i_e(t) \mid)$ and $v(t)$ moves in a bounded region. Observe that the Lissajous curves shown in Fig. 13(c) are very similar to the experimentally measured Lissajous curve (plotted on a semi-log graph) shown in [12]. We conclude as follows:

Since $W(\varphi,\ 0) = 0$, the current $i(t) = W\big(\varphi(t),\ v(t)\big) = 0$ when $v(t) = 0$. This means that the Lissajous curve of $i(t)$ and $v(t)$ on a linear-scale graph passes through the origin and is pinched at the origin as shown in Fig. 13(a).

The voltage-controlled 2-terminal device (85) has the non-volatility property, that is, $\varphi(t)$ does not change during the period when $v(t) = 0$, since $\dfrac{d\varphi}{dt} = 0$ for this period.

- **Example 13. voltage-controlled 2-terminal device**
  Consider next the voltage-controlled 2-terminal device defined by

voltage-controlled 2-terminal device

$$\left.\begin{aligned} i &= W(\varphi,\, v), \\ \frac{d\varphi}{dt} &= v. \end{aligned}\right\} \tag{89}$$

Consider the case where $W(\varphi,\, v)$ is defined by

$$\left.\begin{aligned} W_a(\varphi,\, v) &= W_A - W_B, \\ W_b(\varphi,\, v) &= W_A + W_C, \\ W_c(\varphi,\, v) &= -W_A + W_B, \\ W_d(\varphi,\, v) &= -W_A - W_C, \\ W_e(\varphi,\, v) &= W_A + W_B, \\ W_f(\varphi,\, v) &= W_A - W_C, \\ W_g(\varphi,\, v) &= -W_A - W_B, \\ W_h(\varphi,\, v) &= -W_A + W_C, \end{aligned}\right\} \tag{90}$$

where

$$\left.\begin{aligned} W_A(\varphi,\, v) &\triangleq u(\mid \varphi \mid -0.5)\; u(\mid v \mid -0.5)\; u(v), \\ W_B(\varphi,\, v) &\triangleq u(\mid \varphi \mid -0.5)\; u(\mid v \mid -0.5)\; u(-v), \\ W_C(\varphi,\, v) &\triangleq \{u(\mid \varphi \mid -0.5) - 1\}\; u(\mid v \mid -0.5)\; u(-v), \end{aligned}\right\} \tag{91}$$

and $u(\cdot)$ is the unit step function. Similarly, we consider the case where $W(\varphi,\, v)$ is defined by

$$\left.\begin{aligned} W_i(\varphi,\, v) &= W_D - W_B, \\ W_j(\varphi,\, v) &= W_D + W_C, \\ W_k(\varphi,\, v) &= -W_D + W_B, \\ W_l(\varphi,\, v) &= -W_D - W_C, \\ W_m(\varphi,\, v) &= W_D + W_B, \\ W_n(\varphi,\, v) &= W_D - W_C, \\ W_o(\varphi,\, v) &= -W_D - W_B, \\ W_p(\varphi,\, v) &= -W_D + W_C, \end{aligned}\right\} \tag{92}$$

where

$$W_D(\varphi,\, v) \triangleq -\big\{u(\mid \varphi \mid -0.5)\; -1\big\}\; u\big(\mid v \mid -0.5\big)\; u(v). \tag{93}$$

We also consider the case where $W(\varphi,\, v)$ is defined by

$$\left.\begin{array}{rcl}
W_q(\varphi,\, v) & = & u(\varphi-1)\ u(v-0.5), \\
W_r(\varphi,\, v) & = & u(\varphi-1)\ u(-v-0.5), \\
W_s(\varphi,\, v) & = & -u(\varphi-1)\ u(-v-0.5), \\
W_t(\varphi,\, v) & = & -u(\varphi-1)\ u(v-0.5), \\
W_u(\varphi,\, v) & = & -\big\{u(\varphi-0.5)\ -1\big\}\ u\big(v-0.5\,\big), \\
W_v(\varphi,\, v) & = & -\big\{u(\varphi-0.5)\ -1\big\}\ u\big(-v-0.5\,\big), \\
W_w(\varphi,\, v) & = & \big\{u(\varphi-0.5)\ -1\big\}\ u\big(-v-0.5\,\big), \\
W_x(\varphi,\, v) & = & \big\{u(\varphi-0.5)\ -1\big\}\ u\big(v-0.5\,\big).
\end{array}\right\} \tag{94}$$

Let us apply a sinusoidal voltage source $v_s(t) = r\sin(\omega t)$ for $t \geq 0$. The initial condition is given by $\varphi(0) = 0$. By plotting the Lissajous curve of $i(t)$ and $v(t)$, we obtain the pinched hysteresis loops shown in Figs. 14-16.

Observe that the different combinations are possible depending on whether the direction of the Lissajous curve is clockwise or counterclockwise and in which quadrant the Lissajous curve is located, as shown in Figs. 14-15. Observe also that the Lissajous curves shown in Fig. 16 have only one rectangle (another rectangle is squashed into a line segment) and the direction of the Lissajous curves is either clockwise or counterclockwise. By adding a resistor (10Ω) in parallel to the 2-terminal device, we can check the rotation of the line segment part, since the Lissajous curve turns into one closed curve without a squashed line segment as shown in Fig. 17(b).

We next consider the case where $W(\varphi,\, v)$ is defined by

$$\begin{array}{rcl}
W_y(\varphi,\, v) & = & W_f(\varphi,\, v) + 0.1 \mid v \mid, \\
W_z(\varphi,\, v) & = & \big\{\mid 1.1 - u(\varphi-1) \mid + 5\ u\big(\mid v \mid -8\big)\big\} \mid v \mid .
\end{array} \tag{95}$$

Let us apply a sinusoidal voltage source $v_s(t) = r\sin(\omega t)$ for $t \geq 0$. The initial condition is given by $\varphi(0) = 0$. By plotting the Lissajous curve of $i(t)$ and $v(t)$ (on a linear-scale graph and a semi-log graph), we obtain the interesting curve shown in Fig. 18. This Lissajous curve on a semi-log graph is similar to the experimentally measured one shown in [13]. However, the path direction of the Lissajous curve shown in Fig. 18(d) is different from that of [13].

In order to get the Lissajous curve of [13], we consider a slightly more complex function $W(\varphi,\, v)$ defined by

$$W_\alpha(\varphi,\, v) = u\big(1 - \mid v \mid\big)\ \ \mid v \mid\ \ W_\beta(\varphi,\, v) + 0.3 \mid v \mid + u\big(\mid v \mid -1.7\big), \tag{96}$$

where

$$W_\beta(\varphi,\, v) = \big\{-u(\mid \varphi \mid -0.5)\ -1\big\}\ u(v) + u\big(\mid \varphi \mid -0.5\big)\ u(-v). \tag{97}$$

Let us apply a sinusoidal voltage source $v_s(t) = r\sin(\omega t)$ for $t \geq 0$. The initial condition is given by $\varphi(0) = 0$. By plotting the Lissajous curve of $i(t)$ and $v(t)$ (on a linear-scale graph and a semi-log graph), we obtain the curves shown in Fig. 19. The Lissajous curve on a semi-log graph is similar to the experimentally measured ones shown in [13]. We conclude as follows:

> Since all $W_i(\varphi,\, 0)$ are equal to zero, the current $i(t) = W_i\big(\varphi(t),\, v(t)\big) = 0$ when $v(t) = 0$. This means that the Lissajous curves of $i(t)$ and $v(t)$ on a linear-scale graph pass through the origin and are pinched at the origin as shown in Figs. 14-19, although some portion of the Lissajous curve is squashed into a line segment.

The voltage-controlled 2-terminal device (89) has the non-volatility property, that is, $\varphi(t)$ does not change during the period when $v(t) = 0$ since $\dfrac{d\varphi}{dt} = 0$ for this period.

5 Application of 2-terminal devices and Generic Memristors

In the previous sections we assumed that no state change occurs after setting $v = 0$, i.e., $\tilde{g}(x,\ 0) = 0$ for all x in the case of the generalized 2-terminal devices. If we remove this condition, the state $x(t)$ can exhibit much more interesting behavior. We will show some examples.

5.1 Discrete non-volatile memories

Consider the generalized voltage-controlled 2-terminal devices defined by

generalized voltage-controlled 2-terminal device

$$\left.\begin{array}{rcl} i & = & W(x,\ v), \\ \dfrac{dx}{dt} & = & \tilde{g}(x,\ v), \end{array}\right\} \qquad (98)$$

where i, v, and x denote the terminal current, the terminal voltage, and the state variable of the 2-terminal device, $G(\cdot)$ and $\tilde{g}(\cdot)$ are scalar-valued functions.

Let us first assume that the generalized voltage-controlled 2-terminal device (98) is driven by by the voltage source $v_s(t)$, where the output of the voltage source $v_s(t)$ is set to zero for $t \geq t_0$, that is, $v_s(t) = v(t) = 0$ for $t \geq t_0$.

- **Example 1. non-volatile binary memory**
  Consider the case where $\tilde{g}(x,\ v)$ is given by [1]

$$\tilde{g}(x,\ v) = x - x^3 - h(v), \qquad (99)$$

  <u>which does not satisfy $\tilde{g}(x,\ 0) = 0$ for all x</u> and the scalar function $h(v)$ is defined by

$$h(v) = v - 0.5(\mid v + 1 \mid - \mid v - 1 \mid). \qquad (100)$$

  Let us drive the generalized voltage-controlled 2-terminal device (98) by the voltage source $v_s(t)$, where the output of the voltage source $v_s(t)$ is set to zero for $t \geq t_0$, that is, $v_s(t) = v(t) = 0$ for $t \geq t_0$. Then the state equation for $v = 0$ is given by

$$\frac{dx}{dt} = \tilde{g}(x,\ 0) = x - x^3 = -x(x-1)(x+1). \qquad (101)$$

  It has two asymptotically stable equilibrium points p_1 and p_{-1}, and it also has one unstable equilibrium point p_0. Here, p_1 is situated at $x = 1$, p_{-1} is situated at $x = -1$, and p_0 is situated at $x = 0$. Thus we get the following relation:

■ state of $x(t)$ for $t \gg t_0$

• If $x(t_0) > 0$, then $x(t)$ converges to the asymptotically stable equilibrium point p_1, that is, $x(t) \approx 1$ for $t \gg t_0$.

• If $x(t_0) < 0$, then $x(t)$ converges to the asymptotically stable equilibrium point p_{-1}, that is, $x(t) \approx -1$ for $t \gg t_0$.

• If $x(t_0) = 0$, then $x(t) = 0$, but this point (origin) is unstable.

Next, assume that $W(x,\ v)$ is defined by

$$W(x,\ v) = \mathrm{sgn}(xv). \tag{102}$$

Then $i(t) = W(x(t),\, v(t)) = \mathrm{sgn}\big(v(t)x(t)\big)$. Since $x(t)$ converges to one of the asymptotically stable points or remains at one of the equilibrium points, there exists a real number $M > 0$ such that $\mid x(t) \mid \leq M$ for $t \geq t_0$. Thus, we obtain

$$i(t) = W(x(t),\ v(t)) = \mathrm{sgn}\big(v(t)x(t)\big) = 0 \text{ when } v(t) = 0. \tag{103}$$

To observe the state $x(t)$, we inject a single voltage pulse $v_s(t)$ consisting of sufficiently small amplitude $a > 0$ and sufficiently small width $w > 0$ at $t = t_1 \gg t_0$. Then the state equation for $v = a$ is given by

state equation

$$\frac{dx}{dt} = \tilde{g}(x,\ 0) = x - x^3, \tag{104}$$

where $h(a) = 0$ and $t_1 \leq t \leq t_1 + w \triangleq t_2$. Since Eqs. (101) and (104) are identical, Eq.(104) has the same equilibrium points as those of Eq. (101), that is, two asymptotically stable equilibrium points p_1 and p_{-1} and one unstable equilibrium point p_0. Thus the behavior of the state $x(t)$ is given by

$$\left.\begin{array}{llll} \text{if} & x(t_0) > 0 & \text{then} & x(t) \ \text{ tends to } \ 1, \\ \text{if} & x(t_0) = 0 & \text{then} & x(t) = 0, \\ \text{if} & x(t_0) < 0 & \text{then} & x(t) \ \text{ tends to } \ -1, \end{array}\right\} \tag{105}$$

where $t_0 \ll t_1 \leq t \leq t_2$. However, the origin $x(t) = 0$ is unstable. Thus the current $i(t)$ is given by

$$i(t) = \mathrm{sgn}\big(v(t)x(t)\big) = \left\{\begin{array}{rll} 1 & \text{if} & x(t_0) > 0, \\ 0 & \text{if} & x(t_0) = 0, \\ -1 & \text{if} & x(t_0) < 0, \end{array}\right. \tag{106}$$

where $v_s(t) = v(t) = a > 0$ for $t_1 \leq t \leq t_2$. Thus, the <u>observable</u> current $i(t)$ for the injected single pulse is described by

observable currents for the injected single pulse

$$i(t) = \mathrm{sgn}\big(v(t)x(t)\big) = \pm 1, \tag{107}$$

where $t_1 \leq t \leq t_2$. Therefore, the generalized voltage-controlled 2-terminal device (98) is available for the non-volatile binary memory (see [1], for more details). The results of the computer simulations are shown in Fig. 20, where the injected single pulse is defined by $v_s(t) = 0.1$ for $5 \leq t \leq 5.3$, otherwise $v_s(t) = 0$ and $x(0) = 2.7$. The parameters are given by

$$t_0 = 0,\ t_1 = 5.0,\ t_2 = 5.3,\ a = 0.1,\ w = 0.3. \tag{108}$$

If $x(0) \neq 0$, then we can observe that the current $i(t)$ is equal to 1 or -1 during the period when the injected single pulse is applied to the 2-terminal device (98). Furthermore, the state $x(t)$ is approximately equal to the value $x(5.3)$ even after the pulse signal is turned off. Observe also that the injected single pulse does not affect the behavior of $x(t)$.

Next, we change the state $x(t)$ by applying the second single voltage pulse, which is defined by $v_s(t) = 3$ for $8 \leq t \leq 9$. The results of the computer simulations are shown in Fig. 21. Note that the state $x(t)$ tends to 1 until $t = 9$, and then $x(t)$ tends to -1 by injecting the second single pulse. Also, the current $i(t)$ behaves differently for the first and second pulses.

Finally, we apply a sinusoidal voltage source $v_s(t) = r\sin(\omega t)$ for $t \geq 0$. The initial condition is given by $x(0) = 2.7$. By plotting the Lissajous curve of $i(t)$ and $v(t)$, we obtain the curve shown in Fig. 22(a). Since the sign function $\mathrm{sgn}(z)$ used in Eq. (102) is discontinuous at $z = 0$, the Lissajous curve is not pinched at the origin. If we approximate the sign function by the continuous function $\tanh(kz)$ for $k \gg 1$, then we can observe the pinched hysteresis loop as shown in Fig. 22(b) ($k = 10$). This does not mean that the generalized voltage-controlled 2-terminal device (98) in this example has the normal non-volatile property. However, it does have the non-volatile binary memory property as described above.

- **Example 2. non-volatile multiple-valued memory**
  Consider the case where $\tilde{g}(x,\ v)$ is given by

$$\boxed{\tilde{g}(x,\ v) = \sin(\pi x) - h(v), \qquad (109)}$$

which does not satisfy $\tilde{g}(x,\ 0) = 0$ for all x.

Let us drive the generalized voltage-controlled 2-terminal device (98) by the voltage source $v_s(t)$, where the output of the voltage source $v_s(t)$ is set to zero for $t \geq t_0$, that is, $v_s(t) = v(t) = 0$ for $t \geq t_0$. Then the state equation for $v = 0$ is given by

$$\frac{dx}{dt} = \tilde{g}(x,\ 0) = \sin(\pi x), \tag{110}$$

and it has multiple asymptotically stable equilibrium points at $x = \pm(2n+1)$ and unstable equilibrium points at $x = \pm 2n$, where $n = 0,\ 1,\ 2,\ \cdots$.

We assume next that $W(x,\ v)$ is defined by

$$\boxed{W(x,\ v) \quad = \quad \mathrm{sgn}(v)x. \qquad (111)}$$

Since $x(t)$ converges to one of the asymptotically stable points or remains at one of the equilibrium points, there is a real number $M > 0$ such that $\mid x(t) \mid \leq M$ for $t \geq t_1$. Thus, we obtain

$$\boxed{i(t) = W(x(t),\ v(t)) = 0 \text{ when } v(t) = 0. \qquad (112)}$$

To observe the state $x(t)$, we inject a single voltage pulse $v_s(t)$ consisting of sufficiently small amplitude $a > 0$ and sufficiently small width $w > 0$ at $t = t_1 \gg t_0$. Then the state equation is given by

state equation

$$\frac{dx}{dt} = \tilde{g}(x,\ a) = \sin(\pi x), \tag{113}$$

where $h(a) = 0$ and $t_1 \leq t \leq t_1 + w \triangleq t_2$. Since Eqs. (110) and (110) are identical, Eq. (113) has the same equilibrium points as those of Eq. (110), that is, the asymptotically stable equilibrium points at $\pm(2n+1)$ and the unstable equilibrium point at $\pm 2n$, where $n = 0,\ 1,\ 2,\ \cdots$. Thus the trajectory tends to one of the above asymptotically stable equilibrium points for $t_1 \leq t \leq t_1 + w$, assuming that the initial state $x(t_0)$ is not at the equilibrium point.

Since $v(t) = a > 0$ for $t_1 \leq t \leq t_2$, the observable current $i(t)$ is given by

observable current for the injected single pulse

$$i(t) = W(x(t),\ v(t)) = \mathrm{sgn}(a)\, x(t) = x(t) \approx \pm(2n+1), \tag{114}$$

where $t_1 \leq t \leq t_2$, and $n = 0,\ 1,\ 2,\ \cdots$. Therefore, the generalized voltage-controlled 2-terminal device (98) is available for the non-volatile multiple-valued memory, which is capable of holding m-valued logic values, where m is three or more.

The results of the computer simulations are shown in Fig. 23, where the injected single pulse is defined by $v_s(t) = 0.1$ for $5 \leq t \leq 5.3$, otherwise $v_s(t) = 0$. The parameters are given by

$$t_0 = 0,\ t_1 = 5.0,\ t_2 = 5.3,\ a = 0.1,\ w = 0.3. \tag{115}$$

Observe that the current $i(t)$ takes approximately odd integer values during the period when the injected single pulse (plotted in red) is applied to the 2-terminal device (98). Furthermore, the state $x(t)$ is approximately equal to the value $x(5.3)$ even after the pulse signal is turned off. We can change the state $x(t)$ by applying the second single voltage pulse as stated in Example 1.

Finally, we apply a sinusoidal voltage source $v_s(t) = r\sin(\omega t)$ for $t \geq 0$. The initial condition is given by $x(0) = 6.2$. By plotting the Lissajous curve of $i(t)$ and $v(t)$, we obtain the curve shown in Fig. 24(a). Since the sign function $\mathrm{sgn}(z)$ used in Eq. (111) is discontinuous at $z = 0$, the Lissajous curve is not pinched at the origin. If we approximate the sign function by the continuous function $\tanh(kz)$ for $k \gg 1$, then we can observe the pinched hysteresis loop as shown in Fig. 24(b) ($k = 10$). This does not mean that the generalized voltage-controlled 2-terminal device (98) in this example has the normal non-volatile property. It does, however, have the non-volatile multi-value memory property as described above.

- **Example 3. absolute value limitation**
  Consider the case where $\tilde{g}(x,\ v)$ is given by

$$\tilde{g}(x,\ v) = m(x) - h(v) \tag{116}$$

where

$$m(x) = -x + 0.5\ \{\mid x+1 \mid - \mid x-1 \mid\} = \begin{cases} -x+1, & \text{if } 1 < x, \\ 0, & \text{if } \mid x \mid \leq 1, \\ -x-1, & \text{if } x < -1, \end{cases} \tag{117}$$

Note that the function $\tilde{g}(x,\ v)$ does not satisfy $\tilde{g}(x,\ 0) = 0$ for all x.

Let us drive the generalized voltage-controlled 2-terminal device (98) by the voltage source $v_s(t)$. Assume that the output of the voltage source $v_s(t)$ is set to zero for $t \geq t_0$, that is, $v_s(t) = v(t) = 0$ for $t \geq t_0$. Then the state equation for $v = 0$ is given by

$$\frac{dx}{dt} = \tilde{g}(x,\ 0) = \begin{cases} -x+1, & \text{if } \ 1 < x, \\ 0, & \text{if } \ -1 \mid x \mid \leq 1, \\ -x-1, & \text{if } \ x < -1. \end{cases} \tag{118}$$

Thus the state $x(t)$ for $t \geq t_0$ is given by

- If $x(t_0) > 1$, then $x(t)$ converges to the point $x = 1$ as t tends to the infinity.
- If $\mid x(t_0) \mid \leq 1$, then $x(t) = x(t_0)$.
- If $x(t_0) < -1$, then $x(t)$ converges to the point $x = -1$ as t tends to the infinity.

Assumed next that $W(x,\ v)$ is defined by

$$W(x,\ v) = \mathrm{sgn}(v)\, x. \tag{119}$$

Since $x(t)$ converges to one of the asymptotically stable points or remains $x(t_0)$, there is a real number $M > 0$ such that $\mid x(t) \mid \leq M$ for $t \geq t_0$. Thus, we obtain

$$i(t) = W(x(t),\ v(t)) = \mathrm{sgn}\big(v(t)\big)\, x(t) = 0 \text{ when } v(t) = 0.$$

To observe the state $x(t)$, we inject a single voltage pulse $v_s(t)$ consisting of sufficiently small amplitude $a > 0$ and sufficiently small width $w > 0$ at $t = t_1 \gg t_0$. Then the state equation is given by

state equation

$$\frac{dx}{dt} = \tilde{g}(x,\ a) = \begin{cases} -x+1, & \text{if } \ x > 1, \\ 0, & \text{if } \ \mid x \mid \leq 1, \\ -x-1, & \text{if } \ x < -1, \end{cases} \tag{120}$$

where $h(a) = 0$ and $0 < aw \ll 1$ and $t_0 \ll t_1 \leq t \leq t_1 + w \triangleq t_2$.

Since Eqs. (118) and (120) are identical, the behavior of Eq. (120) is described by

- If $x(t_0) > 1$, then $x(t)$ tends to the point $x = 1$.
- If $\mid x(t_0) \mid \leq 1$, then $x(t) = x(t_0)$.
- If $x(t_0) < -1$, then $x(t)$ tends to the point $x = -1$.

Here, $t_1 \leq t \leq t_1 + w$ and $aw \ll 1$. Thus $x(t)$ is approximated by

$$x(t) \approx \begin{cases} 1 & \text{if } \ x(t_0) > 1, \\ x(t_0) & \text{if } \ \mid x(t_0) \mid \leq 1, \\ -1 & \text{if } \ x(t_0) < -1. \end{cases} \tag{121}$$

The observable current $i(t)$ is approximated by

observable approximated current for the injected single pulse

$$i(t) = W(x(t),\ v(t)) = \mathrm{sgn}(v(t))\, x(t) \approx \begin{cases} 1 & \text{if} \quad x(t_0) > 1, \\ x(t_0) & \text{if} \quad \mid x(t_0) \mid \leq 1, \\ -1 & \text{if} \quad x(t_0) < -1, \end{cases} \tag{122}$$

where $v(t) = a$ for $t_0 \ll t_1 \leq t \leq t_2$. Thus, the generalized voltage-controlled 2-terminal device (98) has the absolute value limitation property for the state $x(t)$.

The results of the computer simulations are shown in Fig. 25, where the injected single pulse is defined by $v_s(t) = 0.1$ for $5 \leq t \leq 5.3$, otherwise $v_s(t) = 0$. The other parameters are given by

$$t_0 = 0,\ t_1 = 5.0,\ t_2 = 5.3,\ a = 0.1,\ w = 0.3. \tag{123}$$

Observe that if $x(0) > 1$, then $i(t)$ is approximately equal to 1 during the period when the injected single pulse (plotted in red) is applied. Observe also that if $\mid x(0) \mid \leq 1$, then $i(t) = x(0)$ during the period when the injected single pulse (plotted in red) is applied. Furthermore, the state $x(t)$ is approximately equal to the value $x(5.3)$ even after the pulse signal is turned off. We can change the state $x(t)$ by applying the second single voltage pulse as shown in Example 1.

Finally, we apply a sinusoidal voltage source $v_s(t) = r\sin(\omega t)$ for $t \geq 0$. The initial condition is given by $x(0) = 2.7$. By plotting the Lissajous curve of $i(t)$ and $v(t)$, we obtain the curve shown in Fig. 24(a). Since the sign function $\mathrm{sgn}(z)$ used in Eq. (119) is discontinuous at $z = 0$, the Lissajous curve is not pinched at the origin. If we approximate the sign function by the continuous function $\tanh(kz)$ for $k \gg 1$, then we can observe the pinched hysteresis loop as shown in Fig. 26(b) ($k = 10$). This does not mean that the generalized voltage-controlled 2-terminal device (98) in this example has the normal non-volatile property. However, it does have the absolute value limitation property as mentioned above.

The generalized 2-terminal devices have the following properties:

- discrete non-volatility property
- absolute value limitation property

We suppose that generalized 2-terminal device (98) has much more interesting properties, if there is no constraint on $\tilde{g}(x,\ v)$.

5.2 Two element oscillators

Consider next the voltage-controlled generic memristor defined by

voltage-controlled generic memristor

$$\left.\begin{aligned} i &= \tilde{G}(\boldsymbol{x})v, \\ \frac{d\boldsymbol{x}}{dt} &= \tilde{\boldsymbol{g}}(\boldsymbol{x},\ v), \end{aligned}\right\} \tag{124}$$

where i, v, and $\boldsymbol{x} = (x_1, x_2, \cdots, x_n) \in \mathbb{R}^n$ indicate the terminal current, the terminal voltage, and the state variables of the memristor, respectively, $\tilde{G}(\cdot)$ is a continuous scalar-valued function, and $\tilde{\boldsymbol{g}} = (\tilde{g}_1, \tilde{g}_2, \cdots, \tilde{g}_n) : \mathbb{R}^n \to \mathbb{R}^n$.

- **Example A. Two-element Duffing oscillator model**

  Assume that

$$\tilde{\boldsymbol{g}}(\boldsymbol{x},\ v) = \big(g_1(\boldsymbol{x},\ v),\ g_2(\boldsymbol{x},\ v)\big) = (z,\ y - y^3 - \gamma z + v), \qquad (125)$$

  where $\boldsymbol{x} = (y,\ z)$ and $\gamma > 0$. Note that $\tilde{\boldsymbol{g}}(\boldsymbol{x},\ v)$ does not satisfy $\tilde{\boldsymbol{g}}(\boldsymbol{x},\ 0) = \mathbf{0}$ for all $\boldsymbol{x}$.

  Let us drive the voltage-controlled generic memristor (124) by the voltage source $v_s(t)$, where the output of the voltage source $v_s(t)$ is set to zero for $t \geq t_0$, that is, $v_s(t) = v(t) = 0$ for $t \geq t_0$. Then the state equation $v = 0$ is described by is given by

$$\left.\begin{array}{rcl} \dfrac{dy}{dt} & = & z, \\ \dfrac{dz}{dt} & = & y - y^3 - \gamma z. \end{array}\right\} \qquad (126)$$

  It has two asymptotically stable equilibrium points at $(y,\ z) = (\pm 1,\ 0)$ and one unstable equilibrium point at the origin. Thus the trajectory $(y(t),\ z(t))$ tends to one of the asymptotically stable equilibrium points, if the initial point satisfies $(x(t_0),\ y(t_0)) \neq (0,\ 0)$.

  Let us drive the voltage-controlled generic memristor (124) by a cosine wave $v_s(t) = r\cos(\omega t)$ for $t \geq t_0$. Then the state equation is equivalent to the Duffing equation:

  Duffing equation

$$\left.\begin{array}{rcl} \dfrac{dy}{dt} & = & z, \\ \dfrac{dz}{dt} & = & y - y^3 - \gamma z + r\cos(\omega t). \end{array}\right\} \qquad (127)$$

  Equation (127) exhibits chaotic behavior if we set $\gamma = 0.2$, $r = 0.3$, and $\omega = 1$.

  Let us define $\tilde{G}(\boldsymbol{x})$ by

$$\tilde{G}(\boldsymbol{x}) = \tilde{G}(y,\ z) = y^2, \qquad (128)$$

  for the passivity of the memristor. Then $i(t) = \tilde{G}(\boldsymbol{x}(t))v(t) = y(t)^2 v(t)$. The observable current $i(t) = y(t)^2 v(t)$ is also chaotic.

  When the trajectory moves in a bounded region of the $(y,\ z)$-plane, there is a real number $M > 0$ such that $\mid y(t) \mid \leq M$ for $t \geq t_0$.

  Then, we obtain

$$i(t) = y(t)^2 v(t) = 0 \text{ when } v(t) = 0.$$

Furthermore, the instantaneous power dissipated by the voltage-controlled generic memristor is given by

$$p(t) = v(t)i(t) = v(t) \times \tilde{G}(\boldsymbol{x}(t))v(t) = y(t)^2 v(t)^2 \geq 0. \tag{129}$$

The energy flow into the memristor from time 0 to t satisfies

$$\int_0^t p(\tau)d\tau \geq 0, \tag{130}$$

for all t, and this memristor is passive.

The state equation of the voltage-controlled generic memristor (124) can be recast into the Duffing equation by the cosine wave drive signal.

The Duffing oscillator can be realized by the only two elements: the passive voltage-controlled generic memristor and the cosine wave source.

We show the chaotic trajectory of Eq. (127) in Fig. 27(left). By plotting the Lissajous curve of $i(t)$ and $v(t)$, we obtain the pinched hysteresis loops shown in Fig. 27(right). The initial condition is given by $y(0) = z(0) = 0$, and the parameters are given by $\gamma = 0.2$, $r = 0.3$, and $\omega = 1$.

It is difficult to observe the internal state $(y(t),\ z(t))$ with the observable current $i(t)$ and the cosine wave $v_s(t) = r\cos(\omega t)$. Therefore, we reconstruct the chaotic attractor by using the current $i(t)$. That is, we plot the trajectories of $\big(i(t),\ i'(t)\big)$ and $\big(i(t),\ i(t-\tau)\big)$ on the two-dimensional plane, where $i'(t) \triangleq di(t)/dt$ and $\tau = 0.7$. The results of the computer simulations are shown in Fig. 28. Observe that the reconstructed attractors are also chaotic, but the shapes of the attractors are slightly different from that shown in Fig. 27(a). For the purpose of comparison, we also reconstruct the chaotic attractor using the internal state $y(t)$. The results of the computer simulations are shown in Fig. 29. The shape of the attractor shown in Fig. 29(a) is very similar to the original chaotic attractor shown in Fig. 27(a).

- **Example B. Two-element Josephson junction circuit model**
  Assume that

$$\tilde{\boldsymbol{g}}(\boldsymbol{x},\ v) = \big(g_1(\boldsymbol{x},\ v),\ g_2(\boldsymbol{x},\ v)\big) = (z,\ -\sin(y) - \beta z + v), \tag{131}$$

where $\boldsymbol{x} = (y,\ z)$ and $\beta > 0$. Note that $\tilde{\boldsymbol{g}}(\boldsymbol{x},\ v)$ does not satisfy $\tilde{\boldsymbol{g}}(\boldsymbol{x},\ 0) = \mathbf{0}$ for all $\boldsymbol{x}$. Let us drive the voltage-controlled generic memristor (124) by the voltage source $v_s(t)$, where the output of the voltage source $v_s(t)$ is set to zero for $t \geq t_0$, that is, $v_s(t) = v(t) = 0$ for $t \geq t_0$. Then the state equation $v = 0$ is equivalent to the circuit model of Josephson junction [15]

circuit model of Josephson junction

$$\left.\begin{aligned} \frac{dy}{dt} &= z, \\ \frac{dz}{dt} &= -\sin(y) - \beta z. \end{aligned}\right\} \tag{132}$$

Equation (132) has multiple asymptotically stable equilibrium points at $(y,\ z) = (\pm 2n\pi,\ 0)$ and unstable equilibrium points at $(y,\ z) = (\pm(2n+1)\pi,\ 0)$, where $n = 0,\ 1,\ 2,\ \cdots$. The trajectory $(y(t),\ z(t))$ tends to one of the asymptotically stable equilibrium points, if the initial point is not initially situated at the equilibrium point.

Let us drive the voltage-controlled generic memristor (124) by a voltage source $v_s(t) = A\sin(\omega t) + D$ for $t \geq t_0$.

forced circuit model of Josephson junction

$$\left.\begin{array}{rcl} \dfrac{dy}{dt} & = & z, \\ \dfrac{dz}{dt} & = & -\sin(y) - \beta z + A\sin(\omega t) + D. \end{array}\right\} \qquad (133)$$

Then Eq. (133) exhibits chaotic behavior, if we set $\beta = 0.3$, $A = 0.8$, $\omega = 0.5$, and $D = 0.28$. Note that this equation is invariant under the following transformation:

$$y \to y + 2\pi. \qquad (134)$$

Let us define $\tilde{G}(\boldsymbol{x})$ by

$$\tilde{G}(\boldsymbol{x}) = \tilde{G}(y,\ z) = z^2. \qquad (135)$$

Then $i(t) = \tilde{G}(\boldsymbol{x}(t))v(t) = z(t)^2 v(t)$. The observable current $i(t) = z(t)^2 v(t)$ is also chaotic, and the voltage-controlled generic memristor (124) is passive.

When the trajectory moves in a bounded region of the $(y,\ z)$-plane, there is a real number $M > 0$ such that $\mid y(t) \mid \leq M$.

Then, we obtain

$$i(t) = z(t)^2 v(t) = 0 \text{ when } v(t) = 0.$$

We conclude the following:

■ The circuit model of Josephson junction is realized by only one passive element, that is, it is realized by the passive voltage-controlled generic memristor.

■ The forced circuit model of Josephson junction can be realized by the two elements: the passive voltage-controlled generic memristor and the sine wave source.

We show the chaotic trajectory of Eq. (133) in Fig. 30(a). Since Eq. (133) is invariant under the transformation: $y \to y + 2\pi$, we plotted the trajectory on the $\big(\mathrm{Mod}[y, 2\pi],\ z\big)$-plane. By plotting the Lissajous curve of $i(t)$ and $v(t)$, we obtain the pinched hysteresis loops shown in Fig. 30(b). The initial condition is given by $y(0) = z(0) = 0$, and the parameters are given by $\beta = 0.3$, $A = 0.8$, $\omega = 0.5$, and $D = 0.28$.

Finally, we reconstruct the chaotic attractor by plotting the trajectories of $\big(i(t),\ i'(t)\big)$ and $\big(i(t),\ i(t-\tau)\big)$ on the two-dimensional plane, where $\tau = 1$. The results of the computer simulations are shown in Fig. 31. Observe that the reconstructed chaotic attractors are chaotic, but the shapes of the attractors

are somewhat different from the original chaotic attractor shown in Fig. 30(a). For the purpose of comparison, we also reconstruct the chaotic attractor using the internal state $z(t)$. The results of the computer simulations are shown in Fig. 32. The shape of the attractor shown in Fig. 32(a) is similar to that shown in Fig. 27(a).

- **Example C. Two-element Mathieu equation model**
  Assume that

$$\tilde{\boldsymbol{g}}(\boldsymbol{x},\ v) = \big(g_1(\boldsymbol{x},\ v),\ g_2(\boldsymbol{x},\ v)\big) = (z,\ (v-a)y), \tag{136}$$

where $\boldsymbol{x} = (y,\ z)$ and $a > 0$. Note that $\tilde{\boldsymbol{g}}(\boldsymbol{x},\ v)$ does not satisfy $\tilde{\boldsymbol{g}}(\boldsymbol{x},\ 0) = \mathbf{0}$ for all $\boldsymbol{x}$.

Let us drive the voltage-controlled generic memristor (124) by the voltage source $v_s(t)$, where the output of the voltage source $v_s(t)$ is set to zero for $t \geq t_0$, that is, $v_s(t) = v(t) = 0$ for $t \geq t_0$. Then the state equation $v = 0$ is given by

$$\left.\begin{array}{rcl} \dfrac{dy}{dt} & = & z, \\ \dfrac{dz}{dt} & = & -ay. \end{array}\right\} \tag{137}$$

It has one equilibrium points at the origin, which is called a center.

Let us drive the voltage-controlled generic memristor (124) by a voltage source $v_s(t) = 2b\cos(2t)$ for $t \geq t_0$, that is, its dynamics is given by

$$\left.\begin{array}{rcl} \dfrac{dy}{dt} & = & z, \\ \dfrac{dz}{dt} & = & -ay + 2b\cos(2t). \end{array}\right\} \tag{138}$$

where b is the parameter.

Then Eq. (124) exhibits a periodic oscillation, if we set $a = 8$ and $b = 5$. Furthermore, if we define $\tilde{G}(\boldsymbol{x})$ by

$$\tilde{G}(\boldsymbol{x}) = \tilde{G}(y,\ z) = y^2, \tag{139}$$

then $i(t) = \tilde{G}(\boldsymbol{x}(t))v(t) = y(t)^2 v(t)$ exhibits a periodic waveform and the voltage-controlled generic memristor (124) becomes passive.

When the trajectory moves in a bounded region of the $(y,\ z)$-plane, that is, there is a real number $M > 0$ such that $\mid y(t) \mid \leq M$.

Then we obtain

$$i(t) = y(t)^2 v(t) = 0 \text{ when } v(t) = 0.$$

Thus, we conclude the following:

The Mathieu equation can be realized by the only two elements: the passive voltage-controlled generic memristor and the cosine wave source.

We show the trajectory of Eq. (138) in Fig. 33(left). By plotting the Lissajous curve of $i(t)$ and $v(t)$, we obtain the pinched hysteresis loops shown in Fig. 33(right). The initial condition is given by $y(0) = 0.1$ and $z(0) = 0$ and the parameters are given by $a = 8$ and $b = 5$.

Finally, we reconstruct the trajectory by plotting the trajectories of $\big(i(t),\ i'(t)\big)$ and $\big(i(t),\ i(t-\tau)\big)$ on the two-dimensional plane, where $\tau = 0.1$. The results of the computer simulations are shown in Fig. 34. We can see that the internal state is oscillating, but the reconstructed trajectory is somewhat different from that shown in Fig. 33(a). For the purpose of comparison, we also reconstruct the trajectory using the internal state $y(t)$. The results of the computer simulations are shown in Fig. 35. The shape of the trajectory shown in Fig. 35(a) is similar to that shown in Fig. 33(a).

We conclude as follows:

- We can observe the internal state through the reconstruction method, although it is not sufficient.
- We suppose that the generic memristor (98) has much more interesting properties when there is no constraint on $\tilde{g}(x,\ v)$.

6 Conclusion

We have defined the 2-terminal devices, which do not belong to the above four classes of memristors, but have the same non-volatile property as the ideal memristor. We have shown that the above 2-terminal devices and the ideal generic memristors can have interesting applications: non-volatile multi-valued memories and two-element chaotic oscillators, if we remove the condition that no state change occurs after the zero driving signal. We have also shown that the 2-terminal devices and the four classes of memristors can exhibit a wide variety of pinched hysteresis loops similar to those measured experimentally. In addition, a variety of Lissajous curves are possible, depending on whether the direction of the Lissajous curve is clockwise or counterclockwise, and which quadrants the Lissajous curve passes through. We believe that many physical systems will be realized or simulated by the four classes of memristors or 2-terminal devices defined in this paper. It is also likely that simpler memristors or 2-terminal devices exist with qualitatively equivalent pinched hysteresis curves.

Acknowledgment

I am grateful to Prof. L. Chua (University of California, Berkeley) for suggesting 15 years ago to find the simplest memristive device that emulates the experimentally measured pinched hysteresis loops.

References

[1] Chua, L. [2011] "Resistance switching memories are memristors", *Appl. Phys. A* **102**, 765-783.

[2] Chua, L. [2015] "Everything you want to know about memristors, but are afraid to ask," *Radioengineering* **24**(2), 319-368.

[3] Chua, L. [2014] "If it's pinched it's a memristor," *Semicond. Sci. Technol.* **29** 104001.

[4] Chua, L.O. [1971] "Memristor–The missing circuit element", *IEEE Trans. Circuit Th.* **CT-18** (5), 507-519.

[5] Chua, L.O. & Kang, S.M. [1976] "Memristive devices and systems," *Proc. IEEE* **64**(2), 209-223.

[6] Chua, L.O. [2012] "The fourth element," *Proc. IEEE* **100**(6), 1920-1927.

[7] Itoh M. & Chua, L.O. [2016] "Parasitic Effects on Memristor Dynamics," *International Journal of Bifurcation and Chaos* **26**(6), (1630014-1)-(1630014-55).

[8] Strukov, D., Snider, G., Stewart, D., & Williams, R.S. [2008] "The missing memristor found," *Nature* **453**, 80-83.

[9] Fujisaki, Y. [2010] "Current Status of Nonvolatile Semiconductor Memory Technology," *Jpn. J. Appl. Phys.* **49**, 100001.

[10] Dong Y., Yu G., McAlpine M.C., Lu W., & Lieber C.M. [2008] "Si/a-Si Core/Shell Nanowires as Nonvolatile Crossbar Switches," *Nano Letters* **8**(2), 386-391.

[11] Beck, A., Bednorz, J.G., Gerber, Ch., Rossel, C. & Widmer D. [2000] "Reproducible switching effect in thin oxide films for memory applications," *Applied Physics Letters* **77**, 139-141.

[12] van der Sluis, P. [2003] "Non-volatile memory cells based on $Zn_xCd_{1-x}S$ ferroelectric Schottky diodes," *Applied Physics Letters* **82**(23), 4089-4091.

[13] Seo, S., Lee, M.J., Seo, D.H., Jeoung, E.J., D.-S. Suh et al. [2004] "Reproducible resistance switching in polycrystalline NiO films," *Appl. Phys. Lett.* **85**(23), 5655-5657.

[14] Oka, T. & Nagaosa N. [2005] "Interfaces of Correlated Electron Systems: Proposed Mechanism for Colossal Electroresistance," *Phys. Rev. Lett.* **95**, 266403.

[15] Itoh M. & Chua, L.O. [2013] "Duality of Memristor Circuits," *International Journal of Bifurcation and Chaos* **23**(1), (1330001-1)-(1330001-50).

A Classification of Memristors

A voltage-controlled memristor can be classified into four classes [2]:

- voltage-controlled ideal memristor

$$\left.\begin{array}{rcl} i & = & G(\varphi)v, \\ \dfrac{d\varphi}{dt} & = & v. \end{array}\right\} \tag{140}$$

- voltage-controlled ideal generic memristor

$$\left.\begin{array}{rcl} i & = & G(x)v, \\ \dfrac{dx}{dt} & = & \hat{g}(x)v. \end{array}\right\} \tag{141}$$

- voltage-controlled generic memristor

$$\left.\begin{array}{rcl} i & = & \tilde{G}(\boldsymbol{x})v, \\ \dfrac{d\boldsymbol{x}}{dt} & = & \tilde{\boldsymbol{g}}(\boldsymbol{x},\ v). \end{array}\right\} \tag{142}$$

- voltage-controlled extended memristor

$$\left.\begin{array}{rcl} i & = & \hat{G}(\boldsymbol{x},\ v)v, \\ & & \mid \hat{G}(\boldsymbol{x},\ 0) \mid < \infty, \\ \dfrac{d\boldsymbol{x}}{dt} & = & \tilde{\boldsymbol{g}}(\boldsymbol{x},\ v). \end{array}\right\} \tag{143}$$

  Here, i, v, φ, and $\boldsymbol{x}$ indicate the terminal current, the terminal voltage, the flux, and the state variable of the voltage-controlled memristor, respectively, $G(\cdot)$, $\tilde{G}(\cdot)$, $\hat{G}(\cdot)$, and $\hat{g}(\cdot)$ are continuous scalar-valued functions, $\boldsymbol{x} = (x_1,\ x_2,\ \cdots,\ x_n) \in \mathbb{R}^n$, and $\tilde{\boldsymbol{g}} = (\tilde{g}_1,\ \tilde{g}_2,\ \cdots,\ \tilde{g}_n) : \mathbb{R}^n \to \mathbb{R}^n$.

Similarly, a current-controlled memristor can be classified into four classes [2]:

- current-controlled ideal memristor

$$\left.\begin{array}{rcl} v & = & R(q)i, \\ \dfrac{dq}{dt} & = & i. \end{array}\right\} \tag{144}$$

- current-controlled ideal generic memristor

$$\left.\begin{array}{rcl} v & = & R(x)i, \\ \dfrac{dx}{dt} & = & \hat{f}(x)i. \end{array}\right\} \tag{145}$$

- current-controlled generic memristor

$$\left.\begin{array}{rcl} v & = & \tilde{R}(\boldsymbol{x})i, \\ \dfrac{d\boldsymbol{x}}{dt} & = & \tilde{\boldsymbol{f}}(\boldsymbol{x},\ i). \end{array}\right\} \tag{146}$$

- current-controlled extended memristor

$$\left.\begin{array}{rcl} v & = & \hat{R}(\boldsymbol{x},\ i)i, \\ & & \mid \hat{R}(\boldsymbol{x},\ 0) \mid < \infty, \\ \dfrac{d\boldsymbol{x}}{dt} & = & \tilde{\boldsymbol{f}}(\boldsymbol{x},\ i). \end{array}\right\} \tag{147}$$

Here, $R(\cdot)$, $\tilde{R}(\cdot)$, $\hat{R}(\cdot)$, and $\hat{f}(\cdot)$ are continuous scalar-valued functions, $\boldsymbol{x} = (x_1,\ x_2,\ \cdots,\ x_n) \in \mathbb{R}^n$, and $\tilde{\boldsymbol{f}} = (\tilde{f}_1,\ \tilde{f}_2,\ \cdots,\ \tilde{f}_n) : \mathbb{R}^n \to \mathbb{R}^n$.

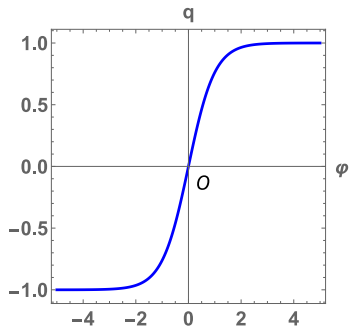

Figure 1: Constitutive relation: $q = g(\varphi) = \tanh(\varphi)$.

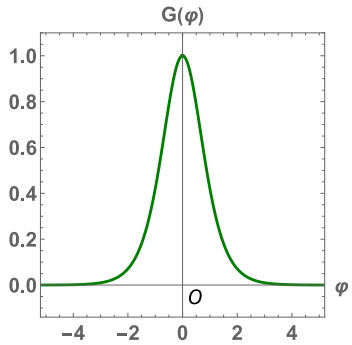

Figure 2: Memductance: $G(\varphi) = \left(1 - \tanh^2(\varphi)\right)$.

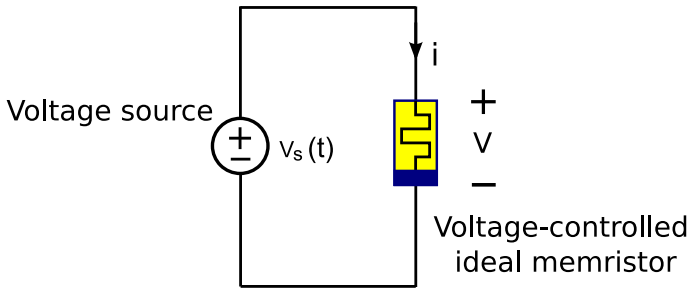

Figure 3: Voltage-controlled ideal memristor driven by the voltage source $v_s(t)$.

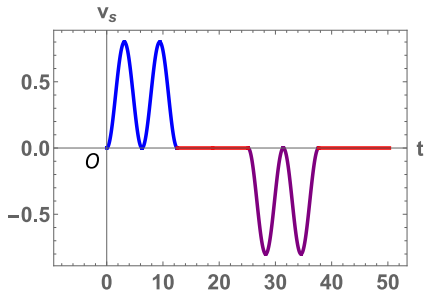

(a) Waveform of $v_s(t)$.

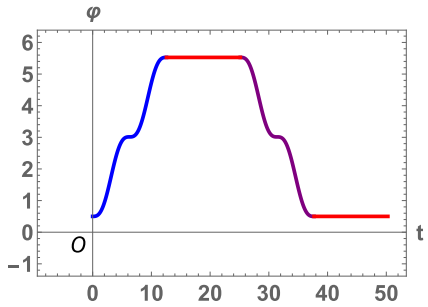

(b) Waveform of $\varphi(t)$.

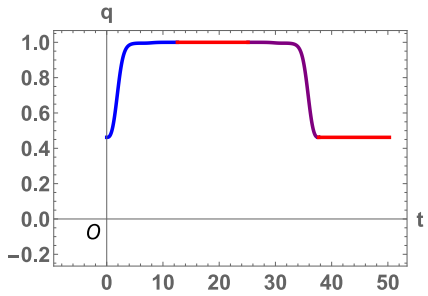

(c) Waveform of $q(t)$.

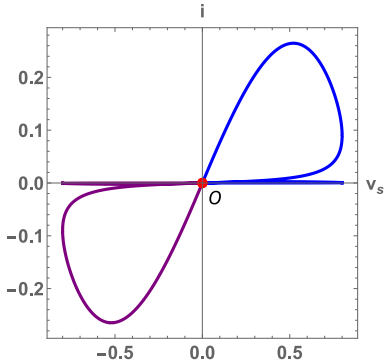

(d) Pinched hysteresis loop.

Figure 4: Non-volatile property of the voltage-controlled ideal memristor (5). (a) Waveform of the voltage source $v_s(t)$. (b)-(c) The values of the flux $\varphi(t)$ and the charge $q(t)$ does not change (plotted in red) during the period when $v_s(t) = 0$. (d) The flux $\varphi(t)$ and the charge $q(t)$ remain unchanged as shown in Figs. 4 (b) and (c) when the Lissajous curve of $v_s(t)$ and $i(t)$ remains at the origin (plotted in red). Note that the response during the period when $v_s(t) = 0$ is the portion of the waveform and trajectory colored in red.

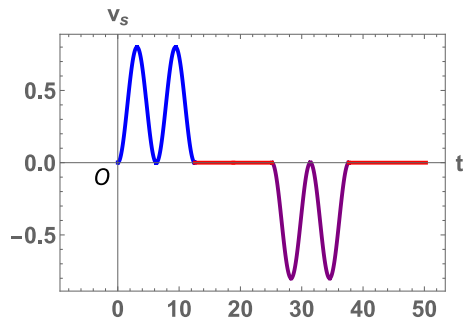

(a) Waveform of $v_s(t)$.

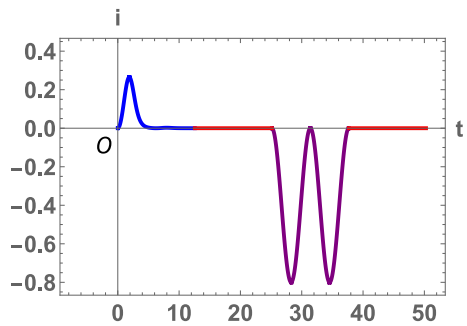

(b) Waveform of $i(t)$.

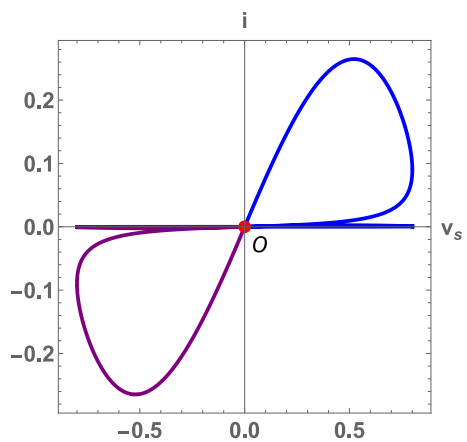

(c) Pinched hysteresis loop.

Figure 5: Waveforms of $v_s(t)$ and $i(t)$ and Lissajous curve of $v_s(t)$ and $i(t)$. (a) Waveform of the voltage source $v_s(t)$. (b) Waveform of the current $i(t)$, which becomes zero during the period when $v_s(t) = 0$. (c) Lissajous curve of $v_s(t)$ and $i(t)$ is pinched at the origin. Note that the response during the period when $v_s(t) = 0$ is the portion of the waveform and trajectory colored in red.

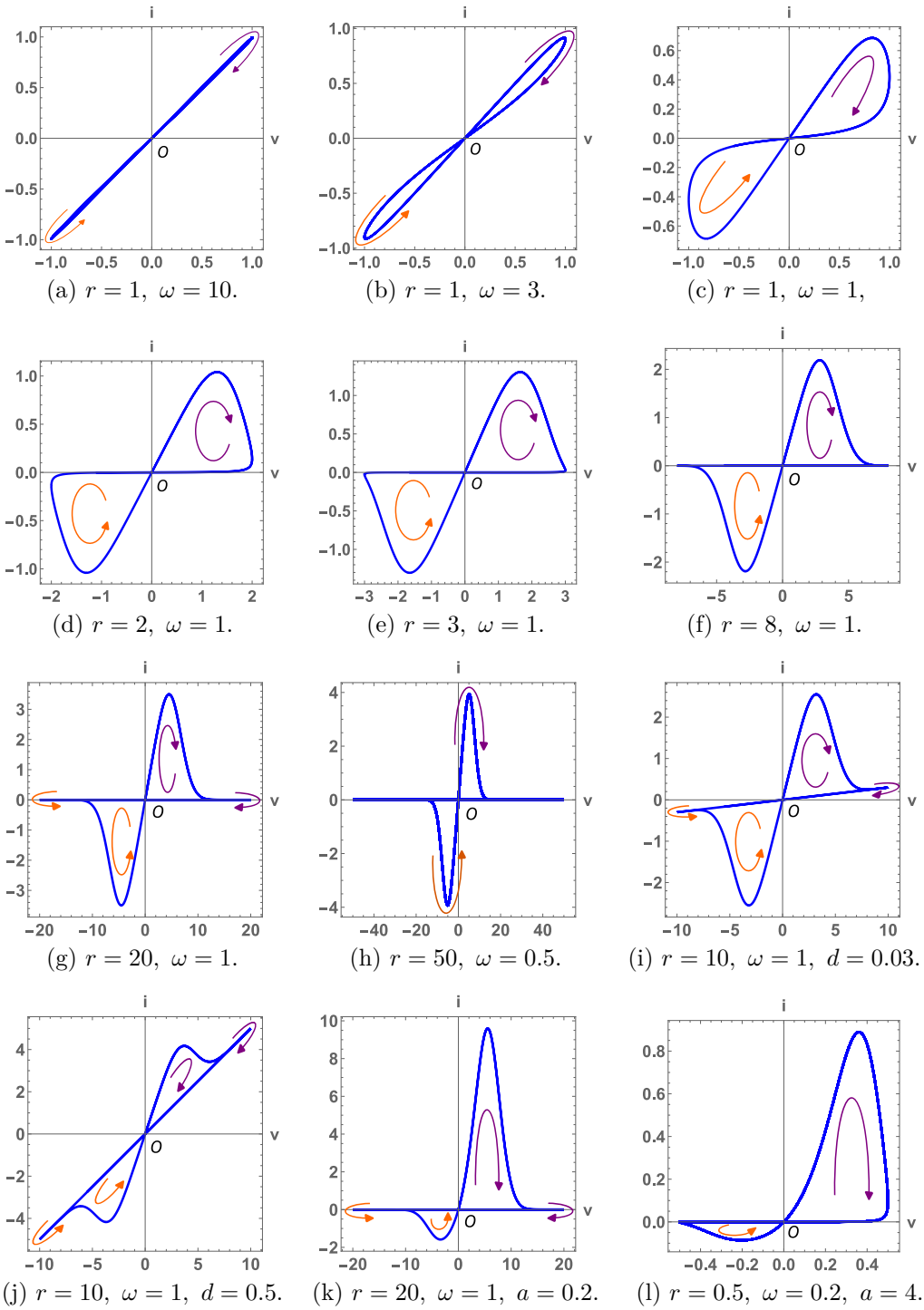

(a) $r = 1,\ \omega = 10.$ (b) $r = 1,\ \omega = 3.$ (c) $r = 1,\ \omega = 1,$

(d) $r = 2,\ \omega = 1.$ (e) $r = 3,\ \omega = 1.$ (f) $r = 8,\ \omega = 1.$

(g) $r = 20,\ \omega = 1.$ (h) $r = 50,\ \omega = 0.5.$ (i) $r = 10,\ \omega = 1,\ d = 0.03.$

(j) $r = 10,\ \omega = 1,\ d = 0.5.$ (k) $r = 20,\ \omega = 1,\ a = 0.2.$ (l) $r = 0.5,\ \omega = 0.2,\ a = 4.$

Figure 6: (a)-(h) Lissajous curves of Eq. (57). (i)-(j) Lissajous curves of Eq. (60). (k)-(l) Lissajous curves of Eq. (62). The Lissajous curve is plotted in purple (resp., orange) when the direction of the curve is clockwise (resp., counterclockwise). The Lissajous curve in Fig. 6(f) is similar to the pinched hysteresis loop shown in [8].

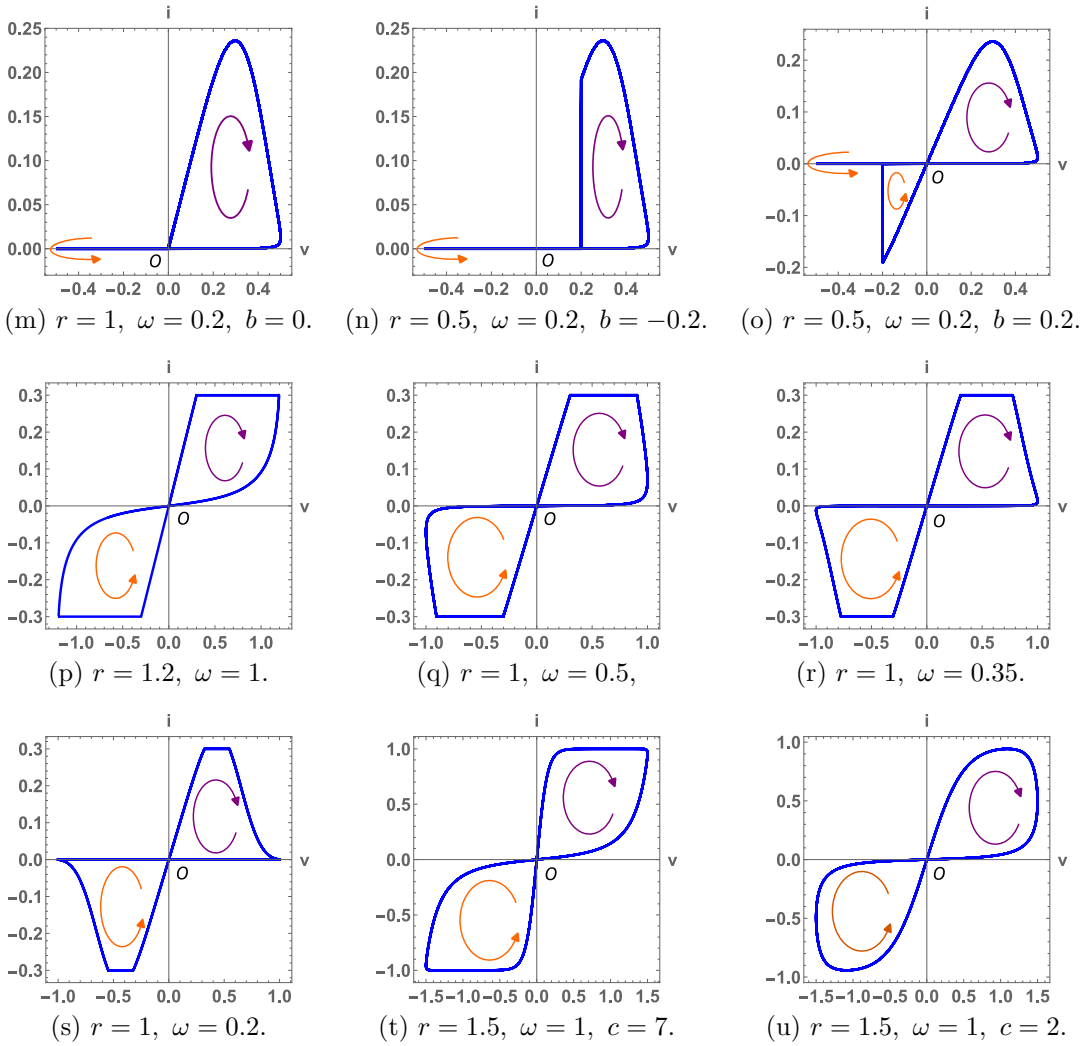

(m) $r = 1,\ \omega = 0.2,\ b = 0.$ (n) $r = 0.5,\ \omega = 0.2,\ b = -0.2.$ (o) $r = 0.5,\ \omega = 0.2,\ b = 0.2.$

(p) $r = 1.2,\ \omega = 1.$ (q) $r = 1,\ \omega = 0.5,$ (r) $r = 1,\ \omega = 0.35.$

(s) $r = 1,\ \omega = 0.2.$ (t) $r = 1.5,\ \omega = 1,\ c = 7.$ (u) $r = 1.5,\ \omega = 1,\ c = 2.$

Figure 7: (m)-(o) Lissajous curves of Eq. (63). (p)-(s) Lissajous curves of Eq. (64). (t)-(u) Lissajous curves of Eq. (67). The Lissajous curve is plotted in purple (resp., orange) when the direction of the curve is clockwise (resp., counterclockwise). Note that a part of the Lissajous curves in Fig. 7(m)-(o) are squashed into a line segment. The Lissajous curve in Fig. 7(p) is very similar to the experimentally measured pinched hysteresis loop shown in [9].

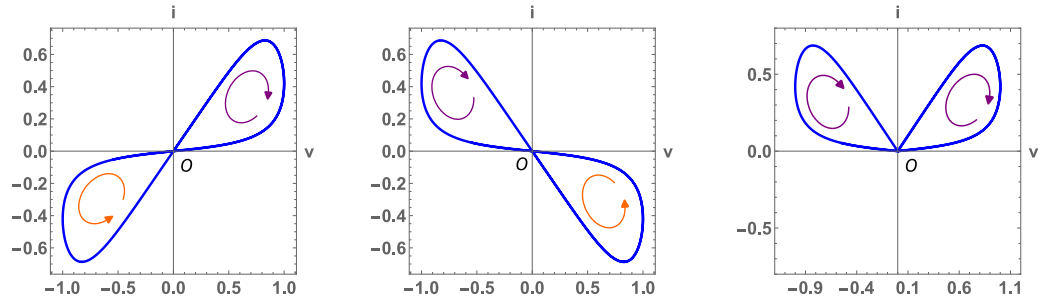

(a) $W_1(\varphi,\, v),\ r = 1,\ \omega = 1.$

(b) $W_2(\varphi,\, v),\ r = 1,\ \omega = 1.$

(c) $W_3(\varphi,\, v),\ r = 1,\ \omega = 1.$

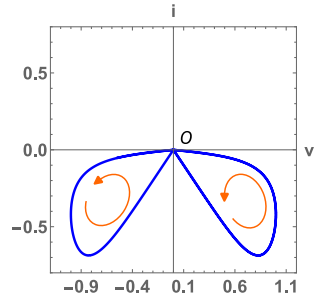

(c) $W_4(\varphi,\, v),\ r = 1,\ \omega = 1.$

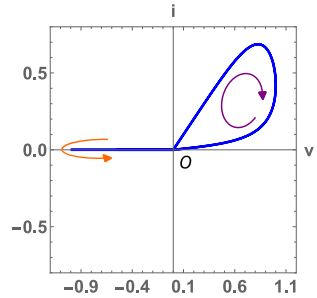

(d) $W_5(\varphi,\, v),\ r = 1,\ \omega = 1.$

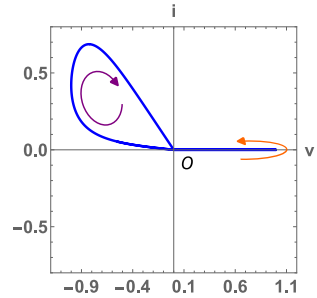

(e) $W_6(\varphi,\, v),\ r = 1,\ \omega = 1.$

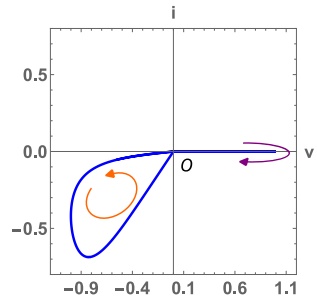

(f) $W_7(\varphi,\, v),\ r = 1,\ \omega = 1.$

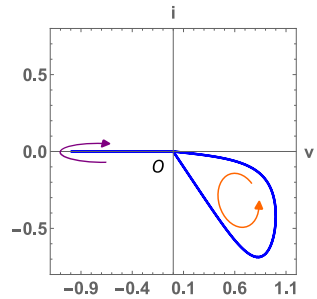

(g) $W_8(\varphi,\, v),\ r = 1,\ \omega = 1.$

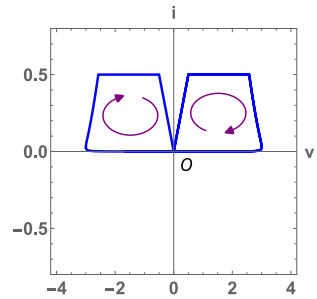

(h) $W_9(\varphi,\, v),\ r = 3,\ \omega = 1.$

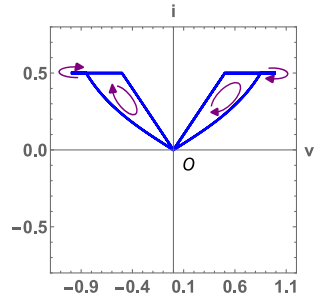

(i) $W_9(\varphi,\, v),\ r = 1,\ \omega = 2.$

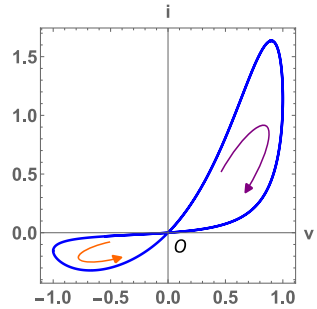

(j) $W_{10}(\varphi,\, v),\ r = 1,\ \omega = 1.$

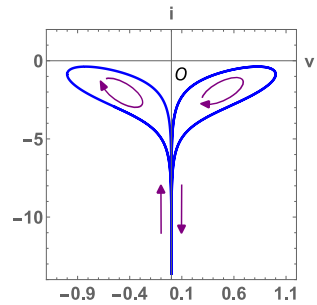

(k) $W_{11}(\varphi,\, v),\ r = 1,\ \omega = 1.$

Figure 8: Lissajous curves of Eq. (70). The Lissajous curve is plotted in purple (resp., orange) when the direction of the curve is clockwise (resp., counterclockwise). Note that a part of the Lissajous curves in Fig 8(d)-(g) are squashed into a line segment.

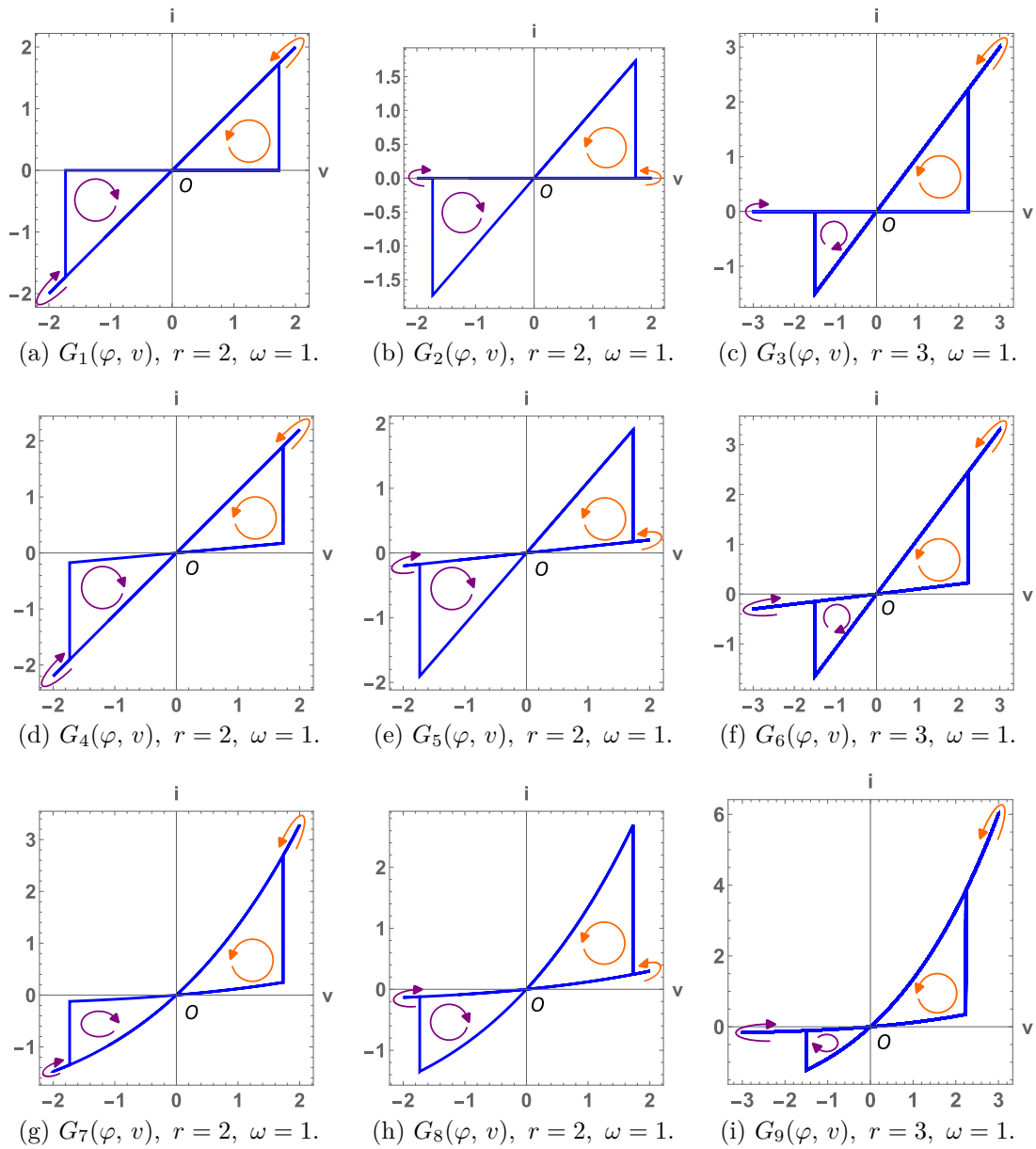

(a) $G_1(\varphi,\, v),\ r = 2,\ \omega = 1.$ (b) $G_2(\varphi,\, v),\ r = 2,\ \omega = 1.$ (c) $G_3(\varphi,\, v),\ r = 3,\ \omega = 1.$

(d) $G_4(\varphi,\, v),\ r = 2,\ \omega = 1.$ (e) $G_5(\varphi,\, v),\ r = 2,\ \omega = 1.$ (f) $G_6(\varphi,\, v),\ r = 3,\ \omega = 1.$

(g) $G_7(\varphi,\, v),\ r = 2,\ \omega = 1.$ (h) $G_8(\varphi,\, v),\ r = 2,\ \omega = 1.$ (i) $G_9(\varphi,\, v),\ r = 3,\ \omega = 1.$

Figure 9: Lissajous curves of Eq. (74). The Lissajous curve is plotted in purple (resp., orange) when the direction of the curve is clockwise (resp., counterclockwise). Observe the difference in the two turning points of the Lissajous curves. The Lissajous curve in Fig. 9(c) is similar to the pinched hysteresis loop shown in [14]. Furthermore, the Lissajous curve in Fig. 9(i) is similar to the pinched hysteresis loop (shoelace plot) shown in [2].

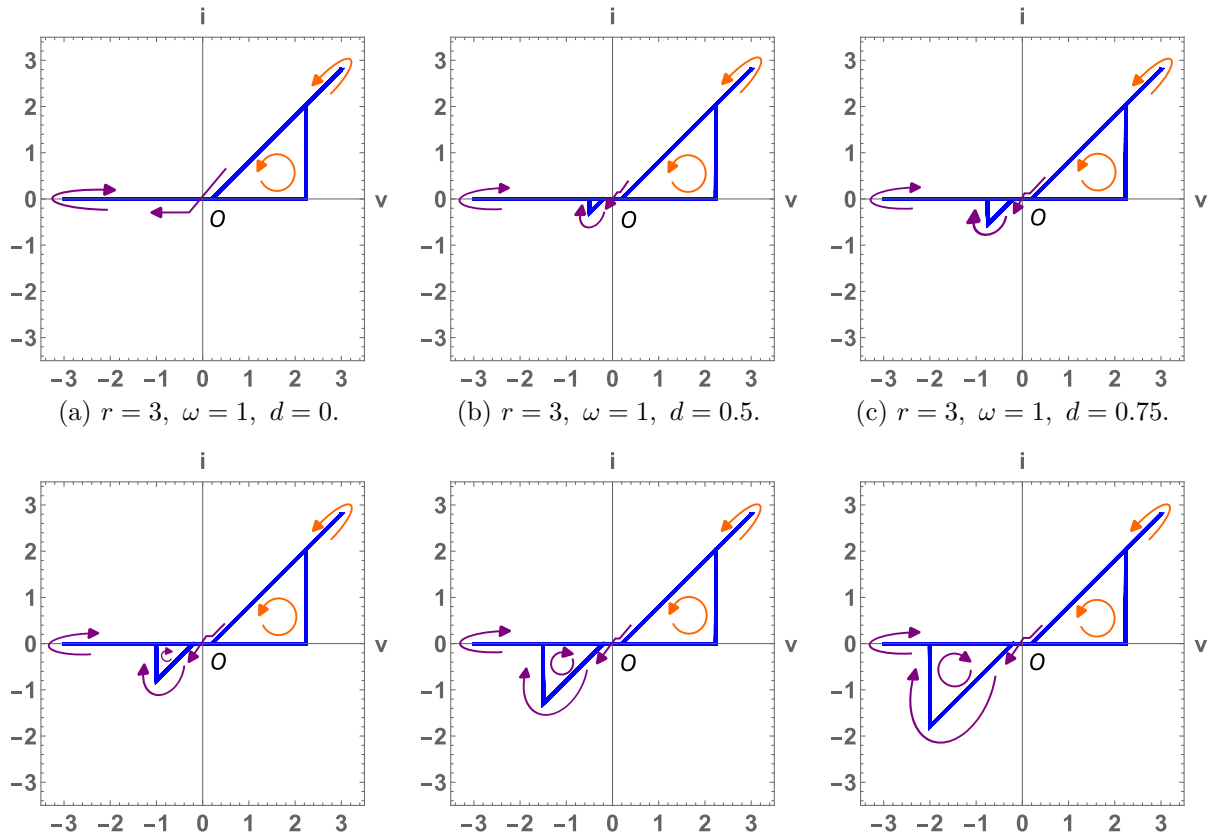

(a) $r = 3,\ \omega = 1,\ d = 0.$ (b) $r = 3,\ \omega = 1,\ d = 0.5.$ (c) $r = 3,\ \omega = 1,\ d = 0.75.$

(d) $r = 3,\ \omega = 1,\ d = 1.$ (e) $r = 3,\ \omega = 1,\ d = 1.5.$ (f) $r = 3,\ \omega = 1,\ d = 2.$

Figure 10: Lissajous curves of Eq. (76). The Lissajous curve is plotted in purple (resp., orange) when the direction of the curve is clockwise (resp., counterclockwise). As the parameter d increases, the newly created triangle becomes larger. Furthermore, a part of the Lissajous curves are squashed into a line segment. Those Lissajous curves are very similar to the experimentally measured pinched hysteresis loops shown in [10].

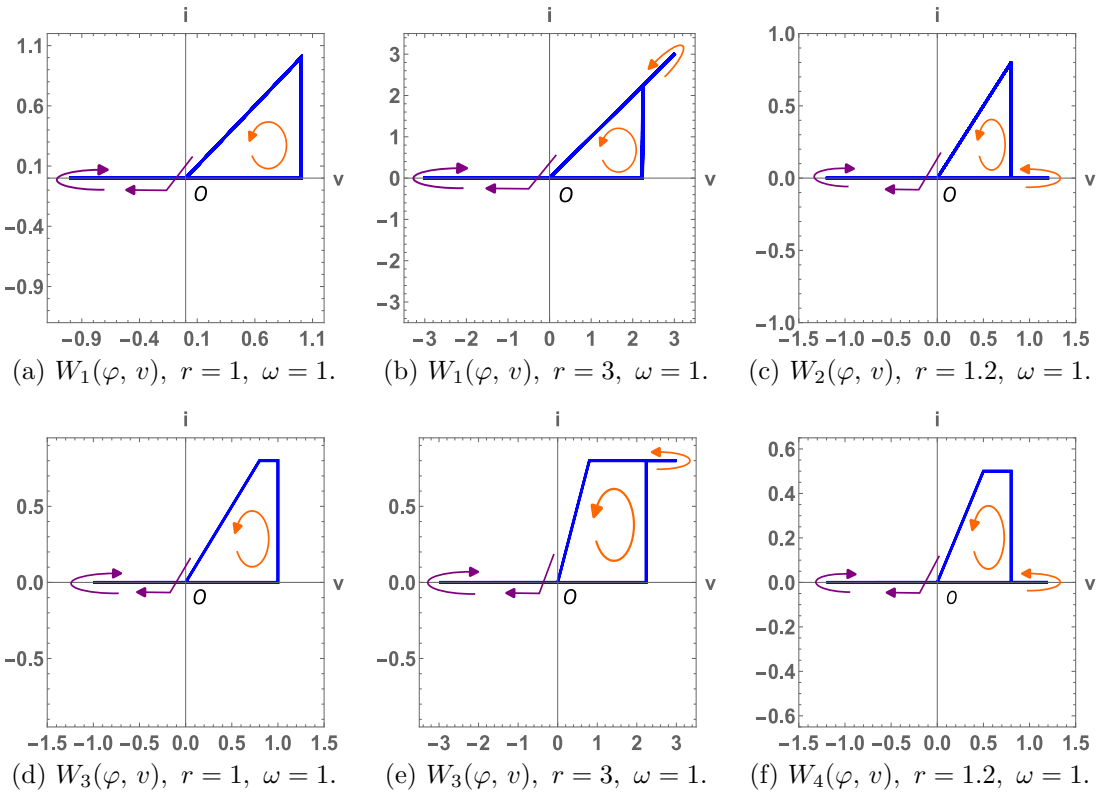

(a) $W_1(\varphi, v),\ r = 1,\ \omega = 1.$ (b) $W_1(\varphi, v),\ r = 3,\ \omega = 1.$ (c) $W_2(\varphi, v),\ r = 1.2,\ \omega = 1.$

(d) $W_3(\varphi, v),\ r = 1,\ \omega = 1.$ (e) $W_3(\varphi, v),\ r = 3,\ \omega = 1.$ (f) $W_4(\varphi, v),\ r = 1.2,\ \omega = 1.$

Figure 11: Lissajous curves of Eq. (79). The Lissajous curve is plotted in purple (resp., orange) when the direction of the curve is clockwise (resp., counterclockwise). Note that the Lissajous curve in the third quadrant is squashed into a line segment. The Lissajous curve in Fig. 11(a) is resembled to the pinched hysteresis loops shown in [8]. Furthermore, the Lissajous curve in Fig. 11(e) is very similar to the experimentally measured pinched hysteresis loops shown in [10].

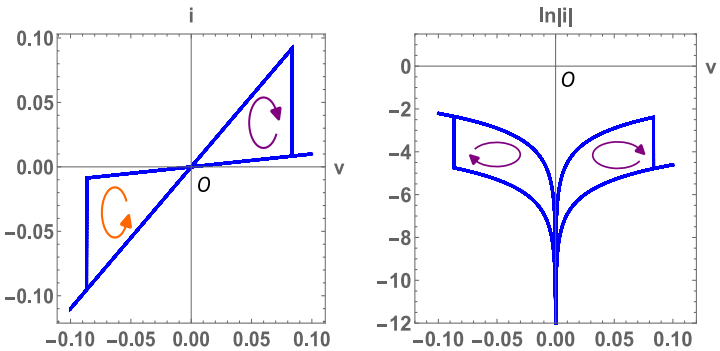

(a) $r = 0.1,\ \omega = 0.3.$ (b) $r = 0.1,\ \omega = 0.3.$

Figure 12: Lissajous curves of Eq. (83). The Lissajous curve is plotted in purple (resp., orange) when the direction of the curve is clockwise (resp., counterclockwise). Note that the Lissajous curve in Fig. 12(b) is plotted on a semi-log graph. Those Lissajous curves are very similar to the experimentally measured Lissajous curves shown in [11].

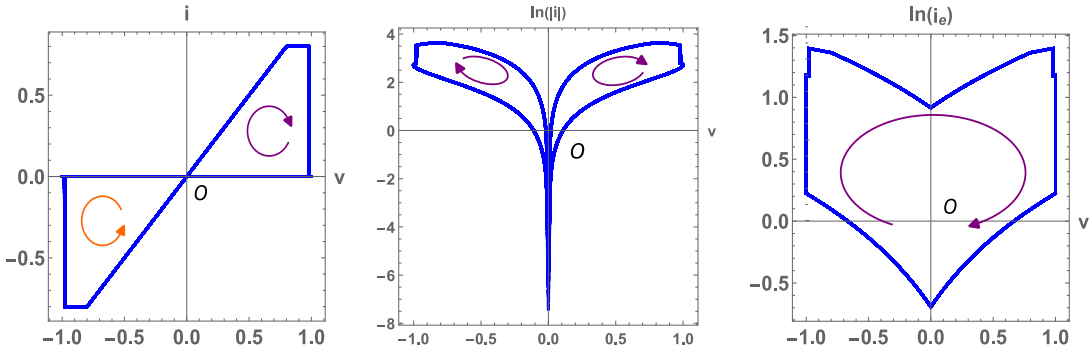

(a) $r = 1,\ \omega = 4.$ (b) $r = 1,\ \omega = 4.$ (c) $r = 1,\ \omega = 4.$

Figure 13: Lissajous curves of Eq. (85). The Lissajous curve is plotted in purple (resp., orange) when the direction of the curve is clockwise (resp., counterclockwise). Note that the Lissajous curves in Fig. 13(b),(c) are plotted on a semi-log graph. Observe that the Lissajous curves in Fig. 13(a), (c) are very similar to the experimentally measured Lissajous curve (plotted on a linear-scale graph and a semi-log graph) shown in [12].

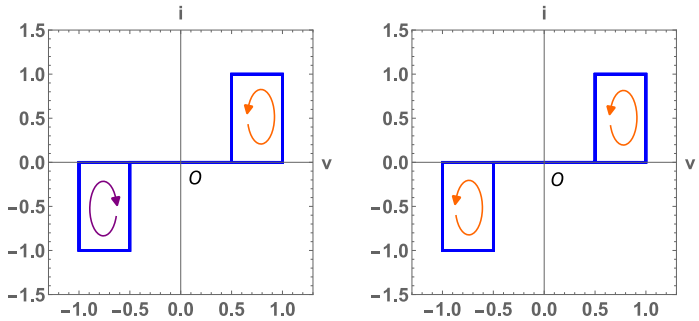

(a) $W_a(\varphi,\, v),\ r = 1,\ \omega = 2.$

(b) $W_b(\varphi,\, v),\ r = 1,\ \omega = 2.$

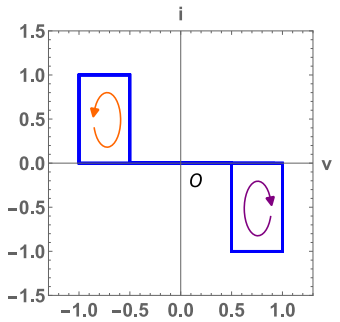

(c) $W_c(\varphi,\, v),\ r = 1,\ \omega = 1.$

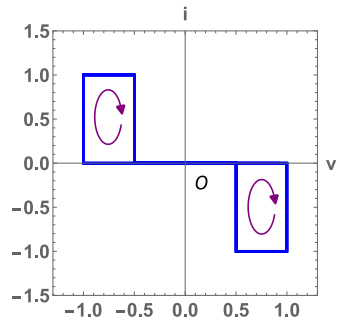

(d) $W_d(\varphi,\, v),\ r = 1,\ \omega = 1.$

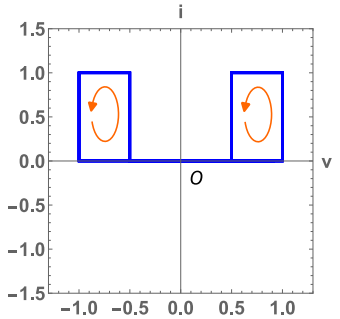

(e) $W_e(\varphi,\, v),\ r = 1,\ \omega = 2.$

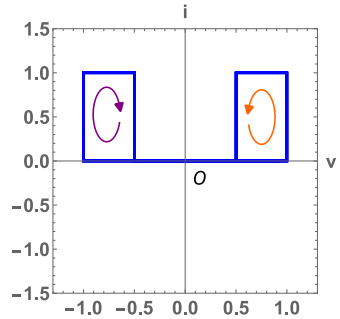

(f) $W_f(\varphi,\, v),\ r = 1,\ \omega = 2.$

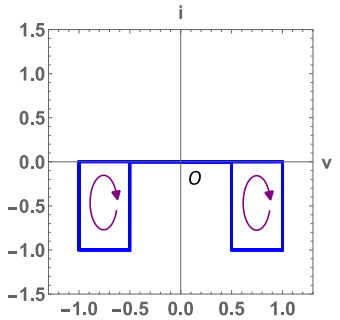

(g) $W_g(\varphi,\, v),\ r = 1,\ \omega = 2.$

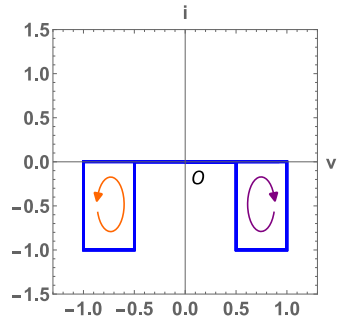

(h) $W_h(\varphi,\, v),\ r = 1,\ \omega = 2.$

Figure 14: Lissajous curves of Eq. (89), which has two rectangles. The Lissajous curve is plotted in purple (resp., orange) when the direction of the curve is clockwise (resp., counterclockwise). Observe that the various combinations are possible, depending on whether the direction of Lissajous curve is clockwise or counterclockwise and which quadrants the Lissajous curve is situated.

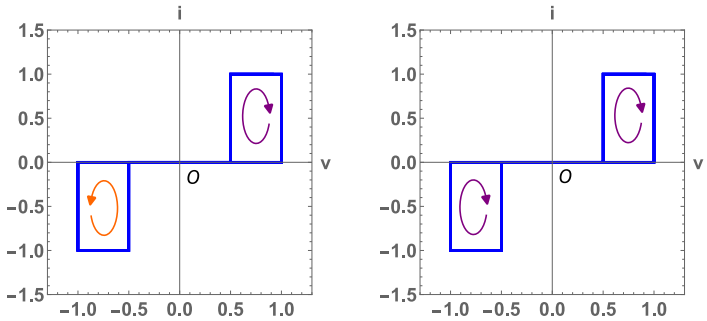

(i) $W_i(\varphi,\, v),\ r = 1,\ \omega = 2.$

(j) $W_j(\varphi,\, v),\ r = 1,\ \omega = 2.$

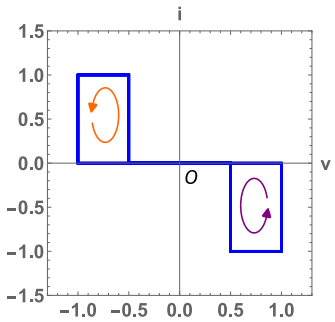

(k) $W_k(\varphi,\, v),\ r = 1,\ \omega = 2.$

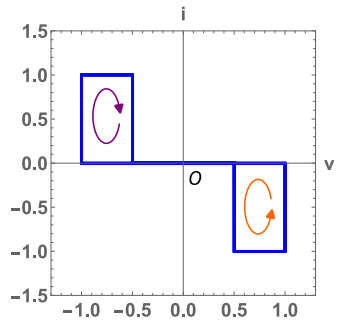

(l) $W_l(\varphi,\, v),\ r = 1,\ \omega = 2.$

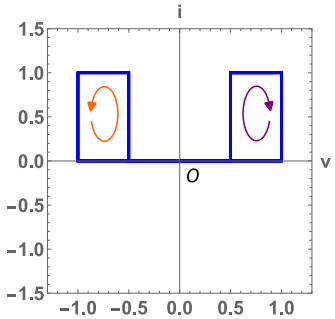

(m) $W_m(\varphi,\, v),\ r = 1,\ \omega = 1.$

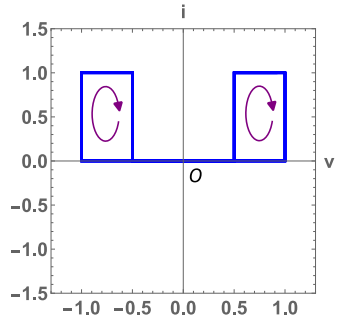

(n) $W_n(\varphi,\, v),\ r = 1,\ \omega = 1.$

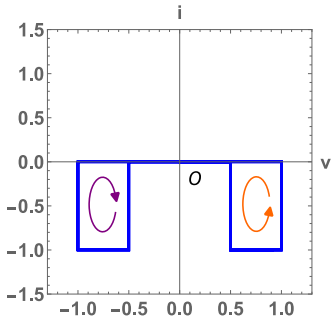

(o) $W_o(\varphi,\, v),\ r = 1,\ \omega = 2.$

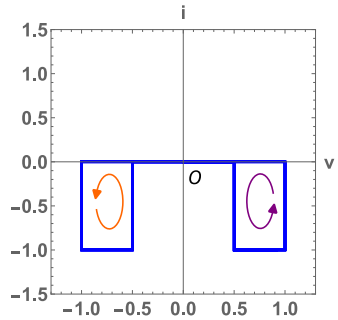

(p) $W_p(\varphi,\, v),\ r = 1,\ \omega = 2.$

Figure 15: Lissajous curves of Eq. (89), which have two rectangles. The Lissajous curve is plotted in purple (resp., orange) when the direction of the curve is clockwise (resp., counterclockwise). Observe that the various combinations are possible, depending on whether the direction of Lissajous curve is clockwise or counterclockwise and which quadrants the Lissajous curve is situated.

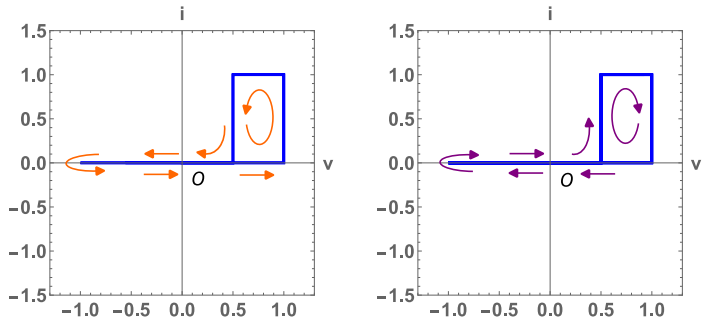

(q) $W_q(\varphi,\, v),\ r = 1,\ \omega = 1.$

(u) $W_u(\varphi,\, v),\ r = 1,\ \omega = 2.$

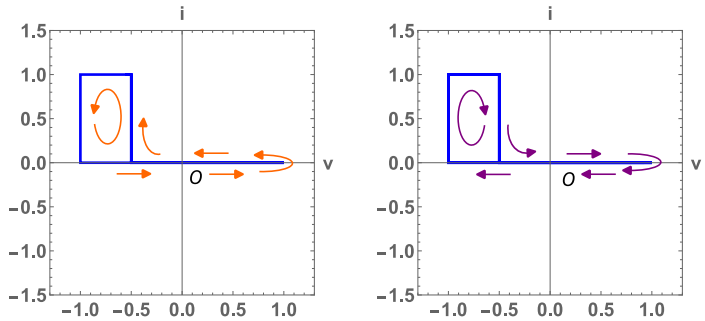

(r) $W_r(\varphi,\, v),\ r = 1,\ \omega = 1.$

(v) $W_v(\varphi,\, v),\ r = 1,\ \omega = 2.$

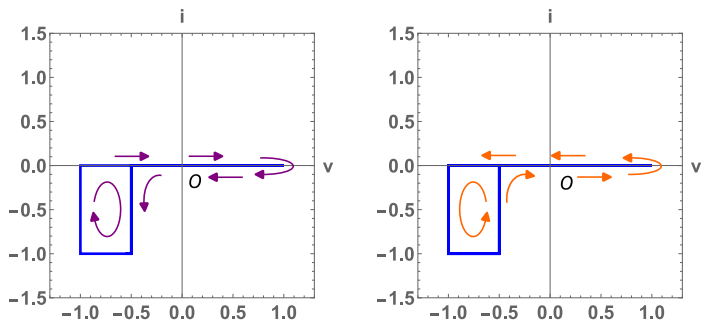

(s) $W_s(\varphi,\, v),\ r = 1,\ \omega = 1.$

(w) $W_w(\varphi,\, v),\ r = 1,\ \omega = 2.$

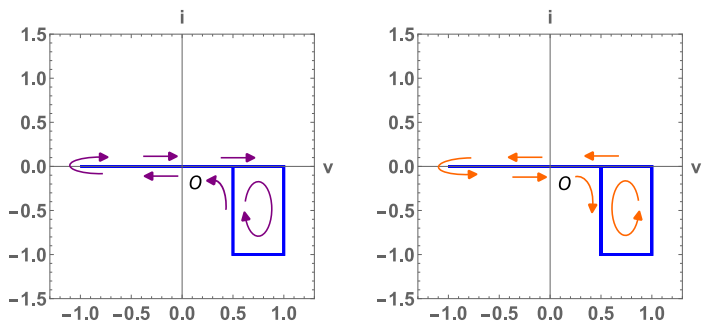

(t) $W_t(\varphi,\, v),\ r = 1,\ \omega = 1.$

(x) $W_x(\varphi,\, v),\ r = 1,\ \omega = 2.$

Figure 16: Lissajous curves of Eq. (89), which have one rectangle (another rectangle is squashed into a line segment). The Lissajous curve is plotted in purple (resp., orange) when the direction of the curve is clockwise (resp., counterclockwise). Observe that the direction of Lissajous curve is either clockwise or counterclockwise.

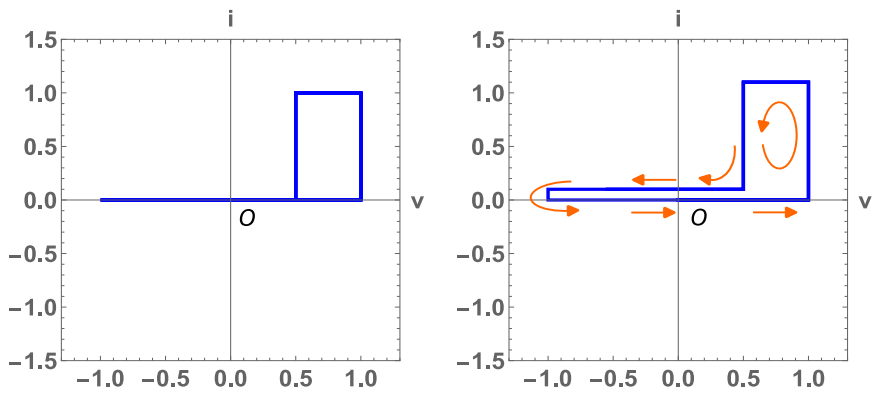

(a) $W_q(\varphi,\, v),\ r = 1,\ \omega = 1.$ (b) $W_q(\varphi,\, v),\ r1,\ \omega = 1.$

Figure 17: Example of the Lissajous curve with one rectangle, which is shown in Fig. 16 (q) (left). By adding a resistor (10Ω) in parallel to the 2-terminal device (89), we can check the rotation of the line segment part, since the Lissajous curve turns into one closed curve without a squashed line segment (right).

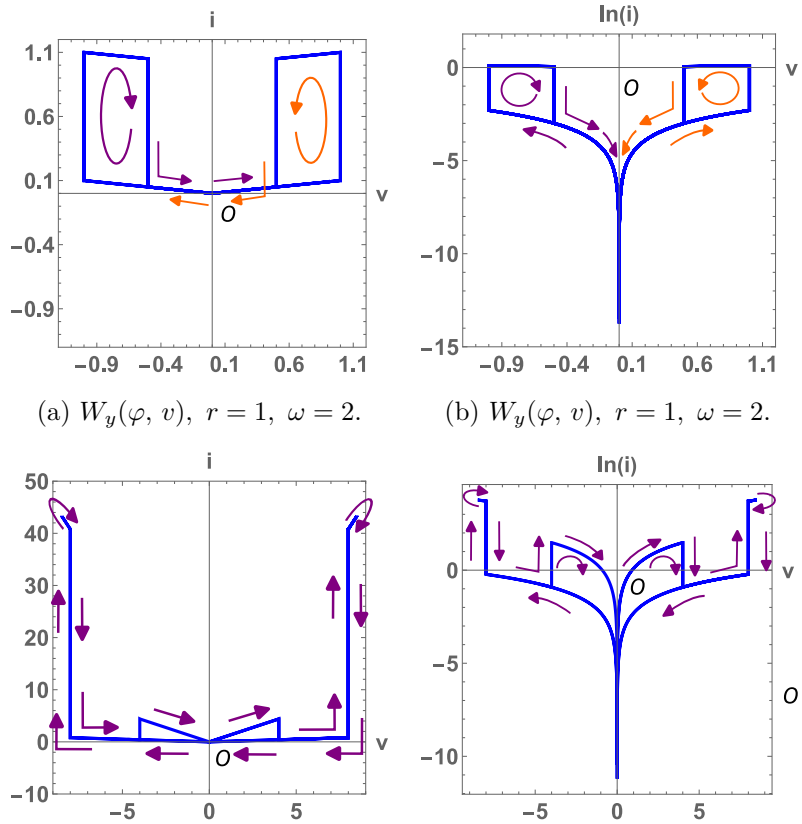

(a) $W_y(\varphi,\, v),\ r = 1,\ \omega = 2.$ (b) $W_y(\varphi,\, v),\ r = 1,\ \omega = 2.$

(c) $W_z(\varphi,\, v),\ r = 8.5,\ \omega = 1.$ (d) $W_z(\varphi,\, v),\ r = 8.5,\ \omega = 1.$

Figure 18: Lissajous curves of Eq. (89). The Lissajous curve is plotted in purple (resp., orange) when the direction of the curve is clockwise (resp., counterclockwise). Note that the Lissajous curves in Fig. 18(b), (d) are plotted on a semi-log graph. They are similar to the experimentally measured ones shown in [13]. However, the path direction of the Lissajous curve in Fig. 18(d) is different from that of [13]

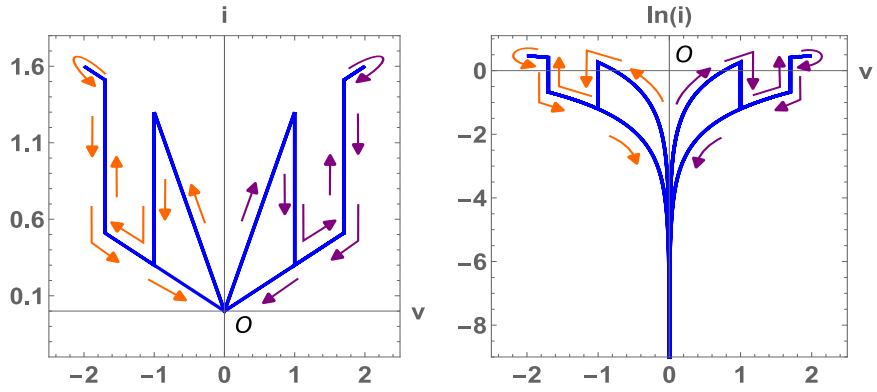

(1) $W_\alpha(\varphi,\, v),\ r = 2,\ \omega = 1.$ (2) $W_\alpha(\varphi,\, v),\ r = 2,\ \omega = 1.$

Figure 19: Lissajous curves for Eq. (96), which are plotted on a linear-scale graph (left) and a semi-log graph (right). This Lissajous curve on the semi-log scale graph is similar to the experimentally measured ones shown in [13].

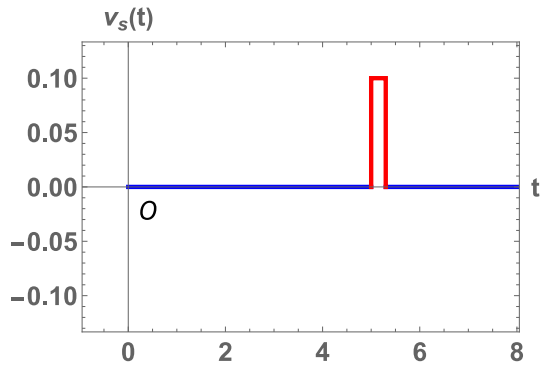

(a) Waveform of the voltage source $v_s(t)$.

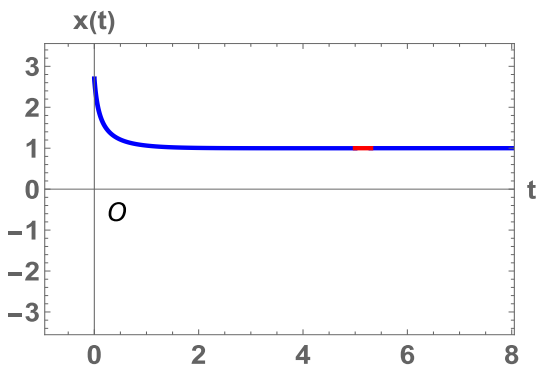

(b) Waveform of $x(t)$ for $x(0) = 2.7$.

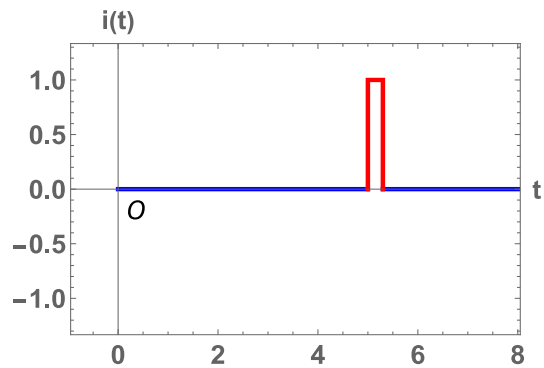

(c) Waveform of $i(t)$ for $x(0) = 2.7$.

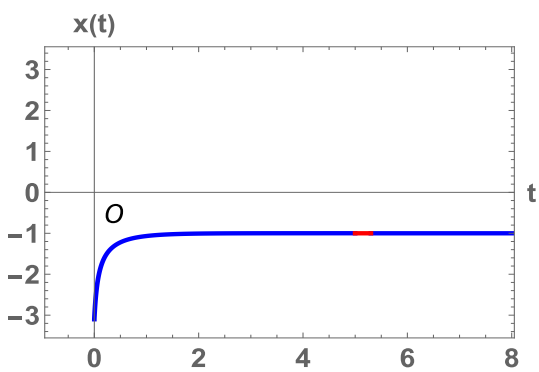

(d) Waveform of $x(t)$ for $x(0) = -3.1$.

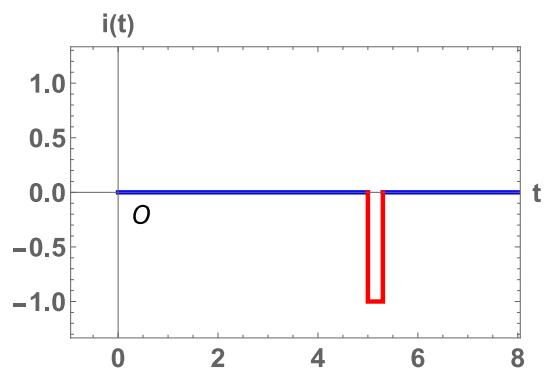

(e) Waveform of $i(t)$ for $x(0) = -3.1$.

Figure 20: Waveforms of the voltage source $v_s(t)$, the state $x(t)$, and the current $i(t)$ for Eq. (99). The injected single pulse (plotted in red in Fig. 20(a)) is defined by $v_s(t) = 0.1$ for $5 \leq t \leq 5.3$, otherwise $v_s(t) = 0$. Observe that the current $i(t)$ is equal to 1 or -1 during the period when the injected single pulse is applied to the 2-terminal device (98), that is, if $x(0) = 2.7$, then $i(t) = 1$ (Fig. 20(b), (c)), and if $x(0) = -3.1$, then $i(t) = -1$ (Fig. 20(d), (e)), where $5 \leq t \leq 5.3$. Furthermore, the state $x(t)$ is approximately equal to the value $x(5.3)$ even after the pulse signal is turned off. Observe also that the injected single pulse does not affect the behavior of $x(t)$. Note that the portion of the waveform colored in red corresponds to the response of the injected single pulse.

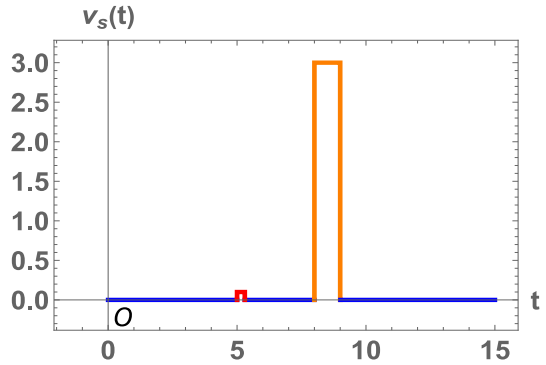

(a) Waveform of the voltage source $v_s(t)$.

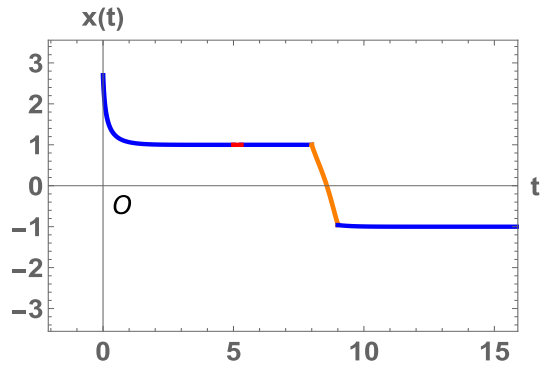

(b) Waveform of the state $x(t)$.

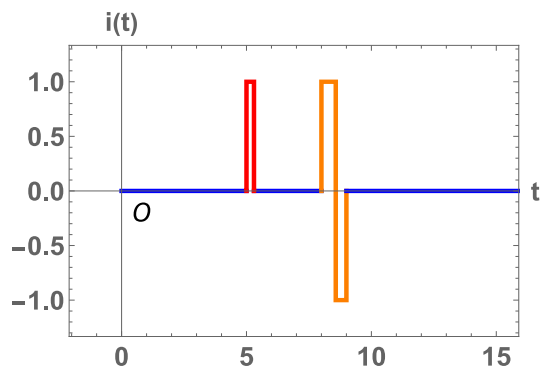

(c) Waveform of the current $i(t)$.

Figure 21: Waveforms of the voltage source $v_s(t)$, the state $x(t)$, and the current $i(t)$. (a) The first pulse (plotted in red) is given by $v_s(t) = 0.1$ for $5 \leq t \leq 5.3$, which is used to observe the state $x(t)$ (see Fig. 20). The second pulse (plotted in orange) is given by $v_s(t) = 3$ for $8 \leq t \leq 9$, which is used to change the state of $x(t)$. (b) The state $x(t)$ tends to 1 until $t = 9$, and then $x(t)$ tends to -1 by injecting the second single pulse. It exhibits the different behavior for the first and second pulses. (c) The current $i(t)$ also exhibits the different behavior for the first and second pulses. Note that the red (resp., orange) portion of the waveform corresponds to the response of the first (resp., second) injected single pulse.

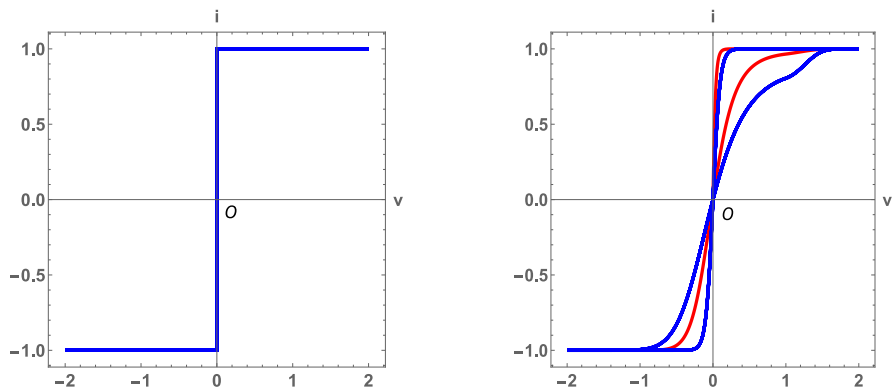

(a) $W(x,\ v) = \mathrm{sgn}(xv),\ r = 2,\ \omega = 1.$ (b) $W(x,\ v) = \tanh(10xv),\ r = 2,\ \omega = 1.$

Figure 22: Lissajous curves of Eq. (98), where the transient curve is colored in red (right). (a) The Lissajous curve is not pinched at the origin. (b) The Lissajous curve shows the pinched hysteresis loop (colored in blue).

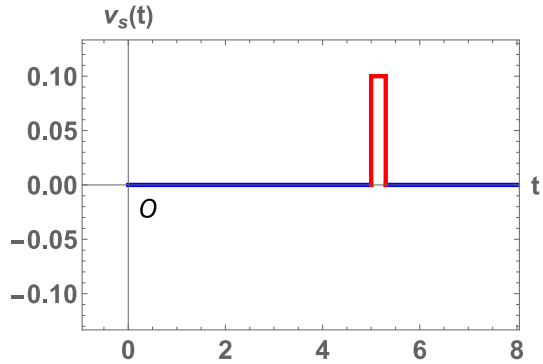

(a) Waveform of the voltage source $v_s(t)$.

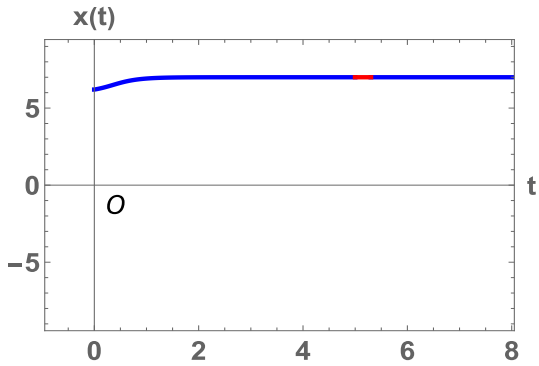

(b) Waveform of $x(t)$ for $x(0) = 6.2$.

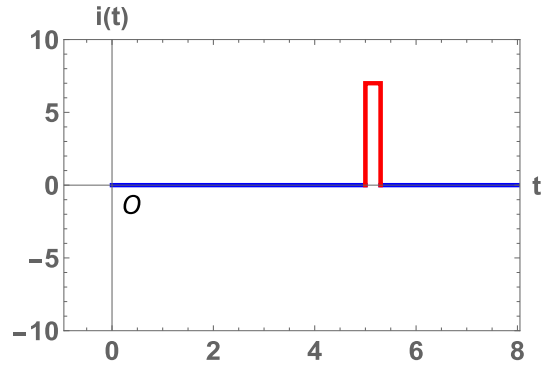

(c) Waveform of $i(t)$ for $x(0) = 6.2$.

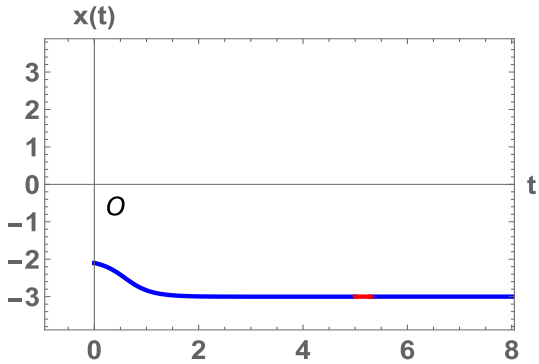

(d) Waveform of $x(t)$ for $x(0) = -2.1$.

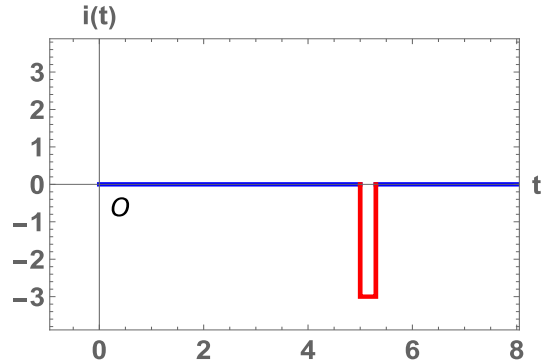

(e) Waveform of $i(t)$ for $x(0) = -2.1$.

Figure 23: Waveforms of the voltage source $v_s(t)$, the state $x(t)$, and the current $i(t)$ for Eq. (109). The injected single pulse (plotted in red in Fig. 23(a)) is defined by $v_s(t) = 0.1$ for $5 \leq t \leq 5.3$, otherwise $v_s(t) = 0$. Observe that the current $i(t)$ takes approximately odd integer values during the period when the injected single pulse is applied to the 2-terminal device (98), that is, if $x(0) = 6.2$, then $i(t) \approx 7$ (Fig. 23(b), (c)) and if $x(0) = -2.1$, then $i(t) \approx -3$ (Fig. 23(d), (e)), where $5 \leq t \leq 5.3$. Furthermore, the state $x(t)$ is approximately equal to the value $x(5.3)$ even after the pulse signal is turned off. Observe also that the injected single pulse does not affect the behavior of $x(t)$. Note that the portion of the waveform colored in red corresponds to the response of the injected single pulse.

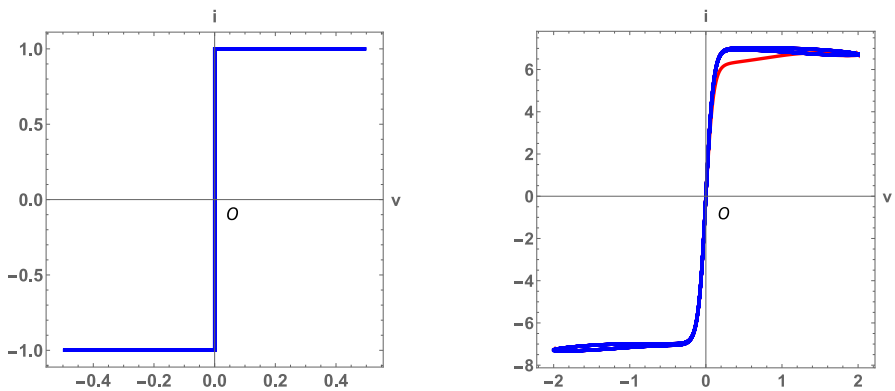

(a) $W(x,\ v) = \mathrm{sgn}(v)x,\ r = 2,\ \omega = 1.$ (b) $W(x,\ v) = \tanh(10v)\,x,\ r = 2,\ \omega = 1.$

Figure 24: Lissajous curves of Eq. (98), where the transient curve is colored in red (right). (a) The Lissajous curve is not pinched at the origin. (b) The Lissajous curve shows the pinched hysteresis loop (colored in blue).

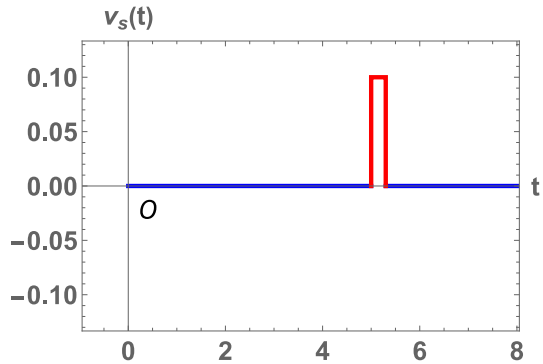

(a) Waveform of the voltage source $v_s(t)$.

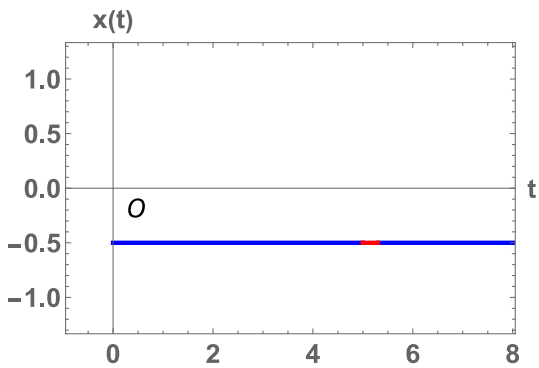

(b) Waveform of $x(t)$ for $x(0) = -0.5$.

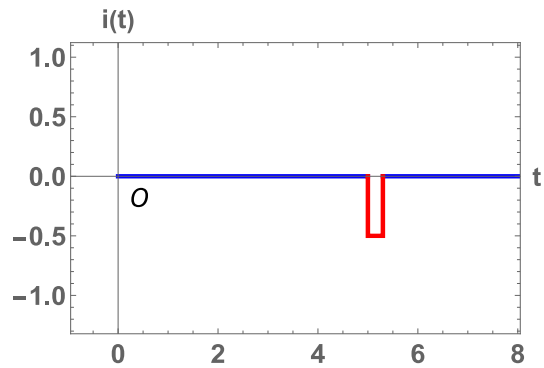

(c) Waveform of $i(t)$ for $x(0) = -0.5$.

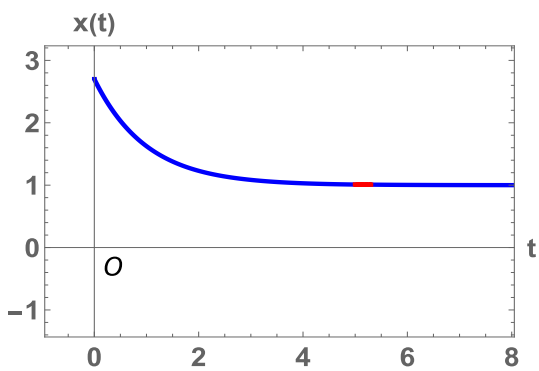

(d) Waveform of $x(t)$ for $x(0) = 2.7$.

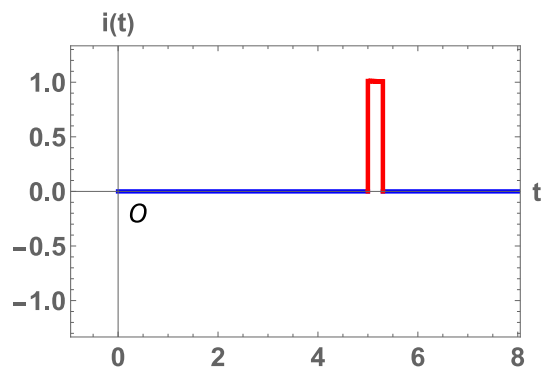

(e) Waveform of $i(t)$ for $x(0) = 2.7$.

Figure 25: Waveforms of the voltage source $v_s(t)$, the state $x(t)$, and the current $i(t)$ for Eq. 116). The injected single pulse (plotted in red in Fig. 25(a)) is defined by $v_s(t) = 0.1$ for $5 \leq t \leq 5.3$, otherwise $v_s(t) = 0$. Observe that if $\mid x(0) \mid \leq 1$, then $i(t) = x(0)$ during the period when the injected single pulse is applied, that is, if $x(0) = -0.5$, then $i(t) = -0.5$ for $5 \leq t \leq 5.3$ (Fig. 25(b), (c)). Observe also that if $x(0) > 1$, then $i(t)$ is approximately equal to 1 during the period when the injected single pulse is applied, that is, if $x(0) = 2.7$, then $i(t) = 1$ for $5 \leq t \leq 5.3$ (Fig. 25(d), (e)). Furthermore, the state $x(t)$ is approximately equal to the value $x(5.3)$ even after the pulse signal is turned off. Observe also that the injected single pulse does not affect the behavior of $x(t)$. Note that the portion of the waveform colored in red corresponds to the response of the injected single pulse.

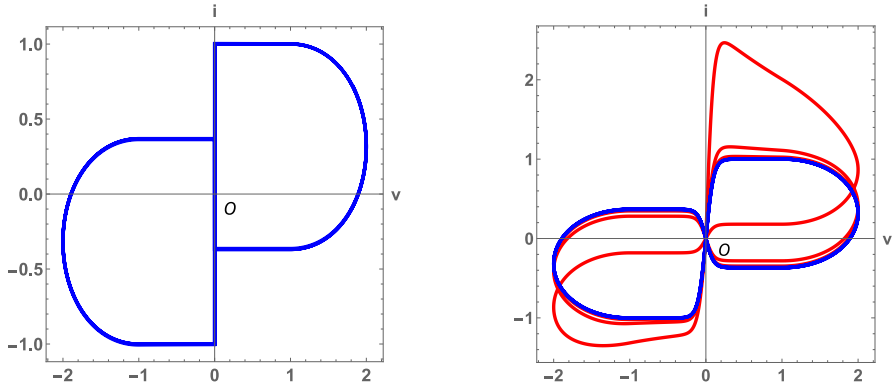

(a) $W(x,\ v) = \mathrm{sgn}(v)x,\ r = 2,\ \omega = 1.$ (b) $W(x,\ v) = \tanh(10v)\,x,\ r = 2,\ \omega = 1.$

Figure 26: Lissajous curves of Eq. (98), where the transient curve is colored in red (right). (a) The Lissajous curve is not pinched at the origin. (b) The Lissajous curve shows the pinched hysteresis loop (colored in blue).

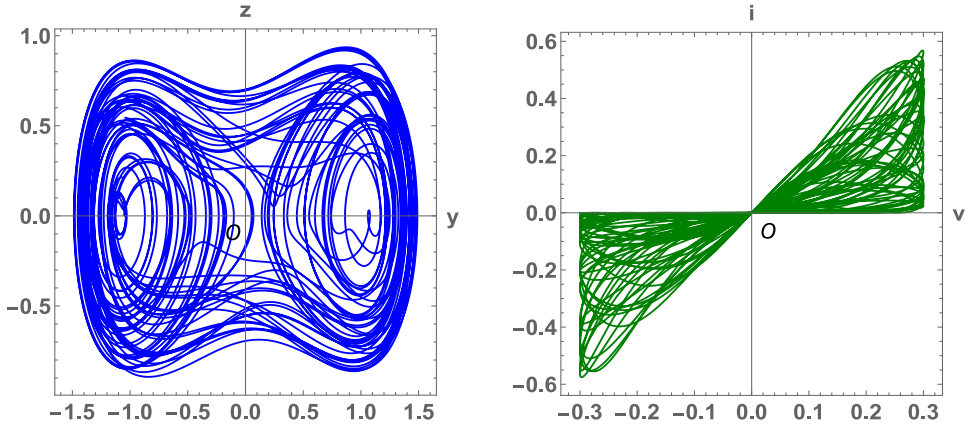

(a) Chaotic trajectory on the $(y,\ z)$-plane. (b) Lissajous curve of $i(t)$ and $v(t)$.

Figure 27: Chaotic trajectory on the $(y,\ z)$-plane and Lissajous curve of $i(t)$ and $v(t)$ of the two-element Duffing oscillator model. The initial condition is given by $y(0) = z(0) = 0$, and the parameters are given by $\gamma = 0.2$, $r = 0.3$, and $\omega = 1$.

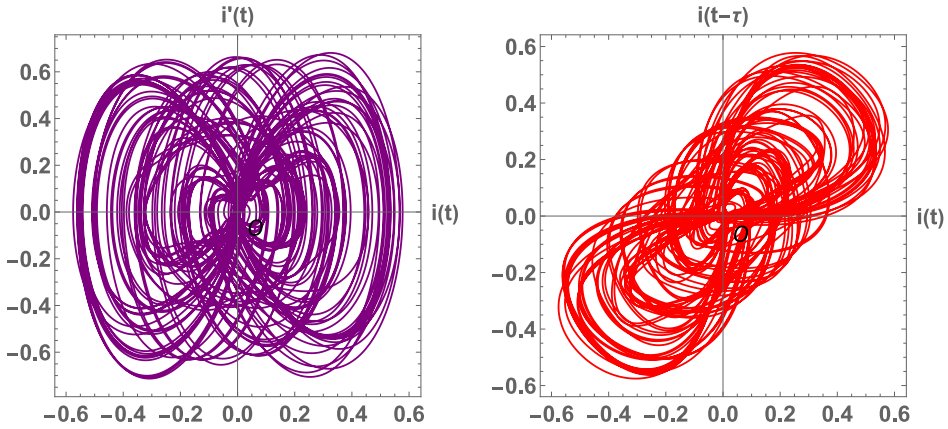

(a) Trajectory of $(i(t),\ i'(t))$. (b) Trajectory of $(i(t),\ i(t-\tau))$.

Figure 28: Reconstructed attractors of the two-element Duffing oscillator model. (a) The trajectory of $(i(t),\ i'(t))$ is plotted. (b) The trajectory of $(i(t),\ i(t-\tau))$ is plotted ($\tau = 0.7$). The initial condition is given by $y(0) = z(0) = 0$, and the parameters are given by $\gamma = 0.2$, $r = 0.3$, and $\omega = 1$.

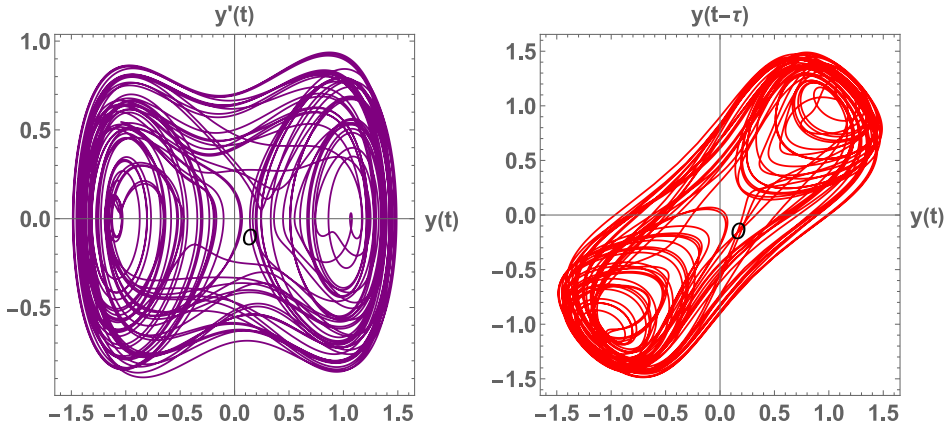

(a) Trajectory of $(y(t),\ y'(t))$. (b) Trajectory of $(y(t),\ y(t-\tau))$

Figure 29: Reconstructed attractors of the two-element Duffing oscillator model. (a) The trajectory of $(y(t),\ y'(t))$ is plotted. (b) The trajectory of $(y(t),\ y(t-\tau))$ is plotted ($\tau = 1.2$). The initial condition is given by $y(0) = z(0) = 0$, and the parameters are given by $\gamma = 0.2$, $r = 0.3$, and $\omega = 1$.

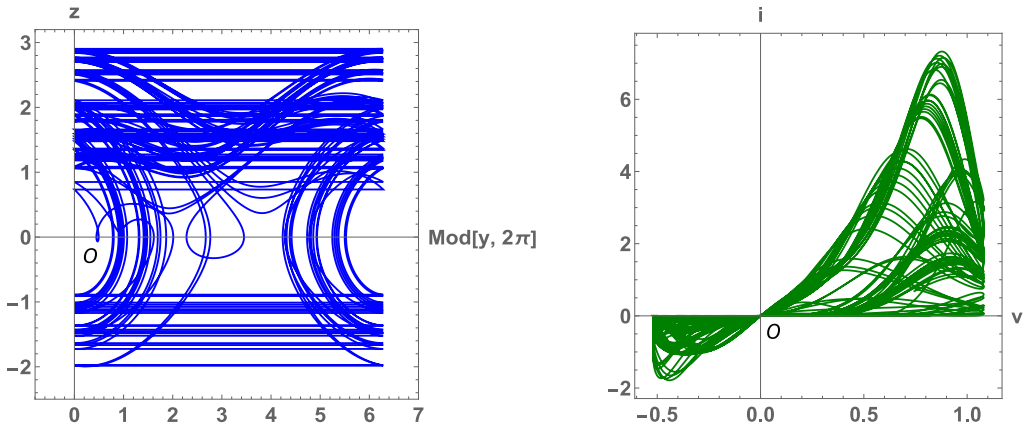

(a) Chaotic trajectory on the $\big(\mathrm{Mod}[y, 2\pi],\ z\big)$-plane. (b) Lissajous curve of $i(t)$ and $v(t)$.

Figure 30: Chaotic trajectory on the $\big(\mathrm{Mod}[y, 2\pi],\ z\big)$-plane and Lissajous curve of $i(t)$ and $v(t)$ of the forced two-element Josephson junction circuit model. The initial condition is given by $y(0) = z(0) = 0$, and the parameters are given by $\beta = 0.3$, $A = 0.8$, $\omega = 0.5$, and $D = 0.28$.

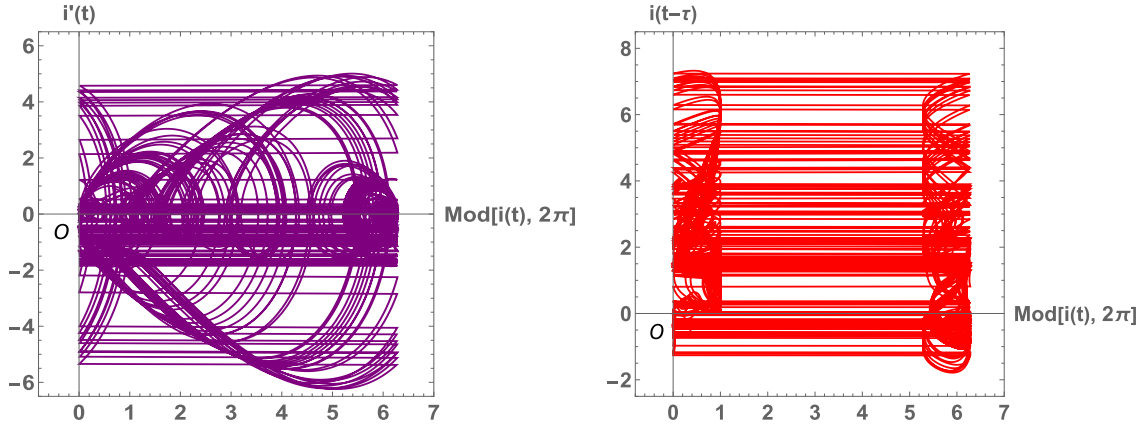

(a) Trajectory of $\big(\mathrm{Mod}[i(t), 2\pi],\ i'(t)\big)$. (b) Trajectory of $\big(\mathrm{Mod}[i(t), 2\pi],\ i(t-\tau)\big)$.

Figure 31: Reconstructed attractors of the forced two-element Josephson junction circuit model. (a) The trajectory of $\big(\mathrm{Mod}[i(t), 2\pi],\ i'(t)\big)$ is plotted. (b) The trajectory of $\big(\mathrm{Mod}[i(t), 2\pi],\ i(t-\tau)\big)$ is plotted ($\tau = 1$) The initial condition is given by $y(0) = z(0) = 0$, and the parameters are given by $\beta = 0.3$, $A = 0.8$, $\omega = 0.5$, and $D = 0.28$.

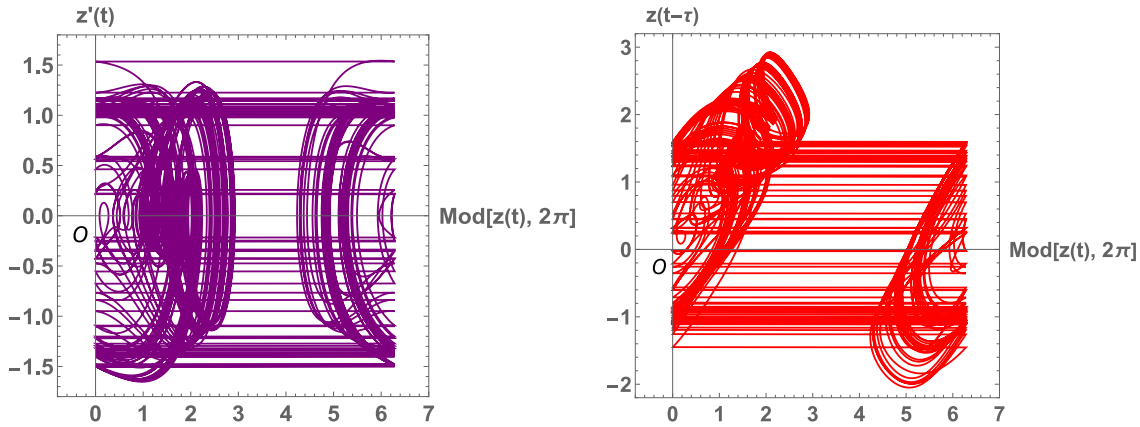

(a) Trajectory of $\big(\mathrm{Mod}[z(t), 2\pi],\ z'(t)\big)$. (b) Trajectory of $\big(\mathrm{Mod}[z(t), 2\pi],\ z(t-\tau)\big)$.

Figure 32: Reconstructed attractors of the forced two-element Josephson junction circuit model. (a) The trajectory of $\big(\mathrm{Mod}[z(t), 2\pi],\ z'(t)\big)$ is plotted. (b) The trajectory of $\big(\mathrm{Mod}[z(t), 2\pi],\ z(t-\tau)\big)$ is plotted ($\tau = 1$) The initial condition is given by $y(0) = z(0) = 0$, and the parameters are given by $\beta = 0.3$, $A = 0.8$, $\omega = 0.5$, and $D = 0.28$.

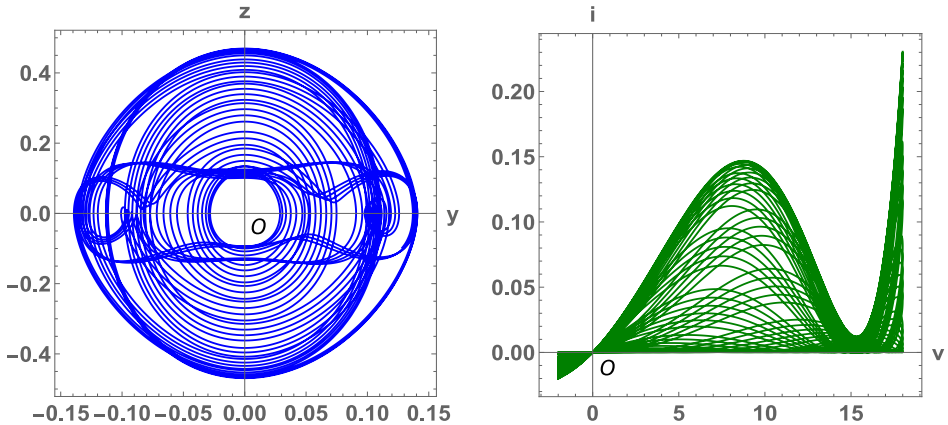

(a) Trajectory on the $(y,\ z)$-plane. (b) Lissajous curve of $i(t)$ and $v(t)$.

Figure 33: Trajectory (left) on the $(y,\ z)$-plane and Lissajous curve of $i(t)$ and $v(t)$ (right) of the forced two-element Mathieu equation model. The initial condition is given by $y(0) = 0.1$ and $z(0) = 0$ and the parameters are given by $a = 8$ and $b = 5$.

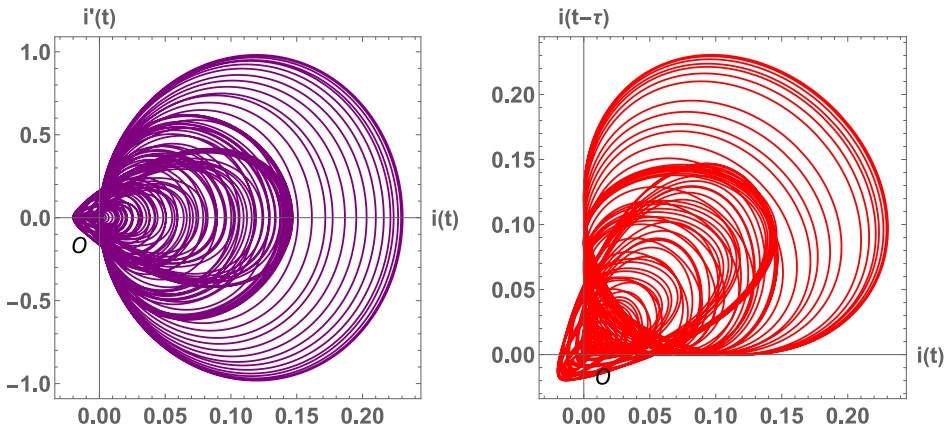

(a) Trajectory of $(i(t),\ i'(t))$. (b) Trajectory of $(i(t),\ i(t-\tau))$.

Figure 34: Reconstructed trajectory of the forced two-element Mathieu equation model. (a) The trajectory of $(i(t),\ i'(t))$ is plotted. (b) The trajectory of $(i(t),\ i(t-\tau))$ is plotted ($\tau = 0.2$) The initial condition is given by $y(0) = 0.1$ and $z(0) = 0$ and the parameters are given by $a = 8$ and $b = 5$.

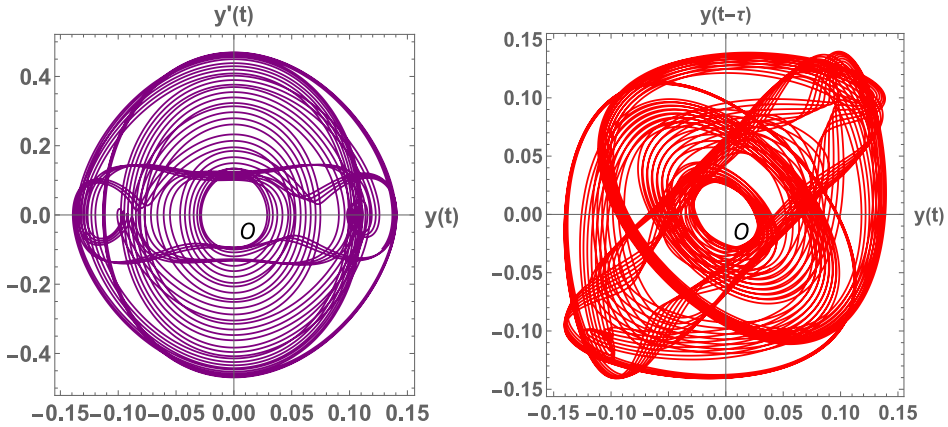

(a) Trajectory of $(y(t),\ y'(t))$. (b) Trajectory of $(y(t),\ y(t-\tau))$

Figure 35: Reconstructed trajectories of the forced two-element Mathieu equation model. (a) The trajectory of $(y(t),\ y'(t))$ is plotted. (b) The trajectory of $(y(t),\ y(t-\tau))$ is plotted ($\tau = 0.5$). The initial condition is given by $y(0) = 0.1$ and $z(0) = 0$ and the parameters are given by $a = 8$ and $b = 5$.